

# Functional cerebral blood volume mapping with simultaneous multi-slice acquisition

## Citation for published version (APA):

Huber, L., Ivanov, D., Guidi, M., Turner, R., Uludag, K., Möller, H. E., & Poser, B. A. (2016). Functional cerebral blood volume mapping with simultaneous multi-slice acquisition. *Neuroimage*, 125, 1159-1168. <https://doi.org/10.1016/j.neuroimage.2015.10.082>

## Document status and date:

Published: 15/01/2016

## DOI:

[10.1016/j.neuroimage.2015.10.082](https://doi.org/10.1016/j.neuroimage.2015.10.082)

## Document Version:

Accepted author manuscript (Peer reviewed / editorial board version)

## Document license:

CC BY-NC-ND

## Please check the document version of this publication:

- A submitted manuscript is the version of the article upon submission and before peer-review. There can be important differences between the submitted version and the official published version of record. People interested in the research are advised to contact the author for the final version of the publication, or visit the DOI to the publisher's website.
- The final author version and the galley proof are versions of the publication after peer review.
- The final published version features the final layout of the paper including the volume, issue and page numbers.

[Link to publication](#)

## General rights

Copyright and moral rights for the publications made accessible in the public portal are retained by the authors and/or other copyright owners and it is a condition of accessing publications that users recognise and abide by the legal requirements associated with these rights.

- Users may download and print one copy of any publication from the public portal for the purpose of private study or research.
- You may not further distribute the material or use it for any profit-making activity or commercial gain
- You may freely distribute the URL identifying the publication in the public portal.

If the publication is distributed under the terms of Article 25fa of the Dutch Copyright Act, indicated by the "Taverne" license above, please follow below link for the End User Agreement:

[www.umlib.nl/taverne-license](http://www.umlib.nl/taverne-license)

## Take down policy

If you believe that this document breaches copyright please contact us at:

[repository@maastrichtuniversity.nl](mailto:repository@maastrichtuniversity.nl)

providing details and we will investigate your claim.

# 1 **Functional Cerebral Blood Volume Mapping with Simultaneous Multi-Slice Acquisition**

2 **Laurentius Huber<sup>a,b\*</sup>, Dimo Ivanov<sup>c</sup>, Maria Guidi<sup>a</sup>, Robert Turner<sup>a</sup>, Kâmil Uludağ<sup>c</sup>, Harald E. Möller<sup>a</sup>, and Benedikt A. Poser<sup>c</sup>**

4 <sup>a</sup> Max Planck Institute for Human Cognitive and Brain Sciences, Leipzig, Germany

5 <sup>b</sup> sFIM, NIMH, NIH, Bethesda, MD, USA

6 <sup>c</sup> Maastricht Brain Imaging Centre, Maastricht University, Maastricht, The Netherlands

8 \*Corresponding author:

9 Laurentius Huber, PhD

10 Section on Functional Imaging Methods, NIMH, National Institutes of Health

11 Building 10, Room 1D80B

12 10 Center Dr. MSC 1148

13 Bethesda, MD 20892-1148

14 Email: Laurentius.Huber@nih.gov

15 Phone: +1 301 402 7298

16

17 Running Title: CBV mapping with SMS VASO

18

19 The body of the text contains 5224 words (with additional 1711 words in references)

## 20 **Highlights:**

- 21 • fMRI with CBV-mapping is combined with a simultaneous multi-slice readout.
- 22 • FOV is increased up to a factor of 4 to enable near whole-brain coverage.
- 23 • High SNR allows high-resolution imaging up to  $1 \times 1 \times 1.2 \text{ mm}^3$ .
- 24 • Higher specificity to GM tissue of CBV-fMRI compared to GE-BOLD is confirmed.

25

## 26 **Abstract**

27 The aim of this study is to overcome the current limits of brain coverage available with  
28 multi-slice echo planar imaging (EPI) for vascular space occupancy (VASO) mapping. By  
29 incorporating simultaneous multi-slice (SMS) EPI image acquisition into slice-saturation slab-  
30 inversion VASO (SS-SI VASO), many more slices can be acquired for non-invasive functional  
31 measurements of blood volume responses.

32 Blood-volume-weighted VASO and gradient echo blood oxygenation level-dependent (GE-  
33 BOLD) data were acquired in humans at 7 T with a 32-channel head coil. SMS-VASO was  
34 applied in three scenarios: **A)** high-resolution acquisition of spatially distant brain areas in  
35 the visuo-motor network (V1/V5/M1/S1); **B)** high-resolution acquisition of an imaging slab  
36 covering the entire M1/S1 hand regions; and **C)** low-resolution acquisition with near whole-  
37 brain coverage.

38 The results show that the SMS-VASO sequence provided images enabling robust detection  
39 of blood volume changes in up to 20 slices with signal readout durations shorter than 150  
40 ms. High-resolution application of SMS-VASO revealed improved specificity of VASO to GM

1 tissue without contamination from large draining veins compared to GE-BOLD in the visual  
2 cortex and in the sensory-motor cortex.

3 It is concluded that VASO fMRI with SMS-EPI allows obtaining a reasonable three-  
4 dimensional coverage not achievable with standard VASO during the short time period  
5 when blood magnetization is approximately nulled. Due to the increased brain coverage  
6 and better spatial specificity to GM tissue of VASO compared to GE-BOLD signal, the  
7 proposed method may play an important role in high-resolution human fMRI at 7 T.

8 **Abbreviations:** BOLD = blood oxygenation level dependent; CBV = cerebral blood volume;  
9 CNR = contrast-to-noise ratio; CSF = cerebrospinal fluid;  $\Delta$ CBV = change in CBV; EPI = echo  
10 planar imaging; fMRI = functional magnetic resonance imaging; GE = gradient echo; GM =  
11 grey matter; MT = magnetization transfer; ROI = region of interest; SNR = signal-to-noise  
12 ratio; SS-SI VASO = slice-selective slab-inversion VASO; TE = echo time; TI = inversion time;  
13 TR = repetition time; VASO = vascular space occupancy.

14 **Keywords:** vascular space occupancy, SS-SI VASO, cerebral blood volume, simultaneous  
15 multi-slice, multi-band, 7 Tesla MRI

## 16 1. Introduction

17 Functional MRI (fMRI) has revolutionized cognitive neuroscience research. The size of  
18 fMRI voxels can now be reduced below one millimeter, approaching the size of  
19 individual cortical layers or columns. Since conventional gradient echo (GE) BOLD fMRI  
20 measures changes in brain activity only indirectly via blood oxygenation changes  
21 (Bandettini, 2012), however, it is limited with respect to its quantifiability and its spatial  
22 specificity.

23 It has been shown (Kim et al., 2013a) that fMRI based on cerebral blood volume (CBV)  
24 can map changes of brain activity with better spatial localization than GE-BOLD signal,  
25 and without contamination by remote draining veins. The most commonly used method  
26 for non-invasive measurements of CBV changes in humans is vascular space occupancy  
27 (VASO) (Lu et al., 2003). Similar to CBV mapping in animals based on injection of contrast  
28 agents, CBV mapping with VASO in humans provides high functional specificity to activity  
29 in neural tissue (Donahue et al., 2006; Huber et al., 2015; Lu et al., 2005). VASO is  
30 particularly attractive at high fields (7 T) due to the increase in image signal-to-noise  
31 ratio and the longer blood  $T_1$  relaxation time, which approaches the vasculature refill  
32 time (Huber et al., 2014c). However, VASO requires image acquisition after an inversion  
33 pulse at the blood magnetization nulling time of approximately  $T_1 \times \ln(2)$ . Thus, if multiple  
34 consecutive slices are acquired after each inversion, they end up with different inversion  
35 times ( $TI$ ), limiting the brain coverage of this method. This is especially problematic at  
36 high resolutions that require acquisition of relatively long echo trains.

1 The acquisition time window and the maximum acquisition duration are usually chosen  
2 such that the uncertainty in the blood nulling time  $\Delta T_1 \times \ln(2)$  is smaller than the variation  
3 of the imaging time  $\Delta T_I$  (Lu et al., 2004; Scouten and Constable, 2007). Considering that  
4 the variation of blood  $T_1$  with oxygenation state and haematocrit is in the order of 200  
5 ms (Grgac et al., 2012; Rane and Gore, 2013; Zhang et al., 2012), all VASO data should be  
6 acquired within this corresponding time interval. This limits the number of slices that  
7 can be acquired with conventional EPI to be not greater than five (Huber et al., 2014a;  
8 Huber et al., 2014c; Scouten and Constable, 2007).

9 Previous studies suggest that VASO coverage can be increased by combining VASO spin  
10 preparation with advanced readout techniques such as three-dimensional (3D) GRASE  
11 (Donahue et al., 2009; Poser and Norris, 2007, 2009). However, the long acquisition time  
12 required for 3D GRASE and the shorter tissue  $T_2$  at high field strengths can induce  
13 through-plane blurring due to  $T_2$  decay. In high-resolution fMRI, the short  $T_2$  can also  
14 introduce limitations with respect to the echo-train length, the number of acquired  
15 slices, or spin echo (SE) BOLD signal contamination in VASO. This can be improved by  
16 shortening the acquisition window, i.e., by shortening the echo-train length, by means of  
17 in-plane parallel imaging. However, the considerable k-space undersampling with high  
18 parallel imaging acceleration factors incurs losses in signal-to-noise ratio (SNR).  
19 Furthermore, the numerous refocusing radiofrequency (RF) pulses can introduce  
20 unacceptable additional energy deposition in sequences limited by specific absorption  
21 rate (SAR) restrictions.

22 Alternatively, VASO coverage can be increased by combining VASO spin preparation with  
23 multi-shot 3D readout strategies (Cretti et al., 2013; Hua et al., 2013). However, since in  
24 this acquisition scheme different parts of k-space are acquired after separate excitation  
25 pulses, only the k-space center is acquired at the blood-nulling time. This implies that  
26 the high spatial frequencies (outer k-space lines, respectively) will be weighted by blood  
27 flow effects in addition to the weighting from blood volume changes, which can  
28 introduce inaccuracies in high-resolution fMRI.

29 Recently, simultaneous multi-slice imaging (SMS) with multi-band (MB) excitation was  
30 developed to boost the brain coverage of data acquisition within a given acquisition  
31 period (Feinberg et al., 2010; Moeller et al., 2010; Setsompop et al., 2012a). The use of  
32 SMS-EPI can multiply the number of acquired slices during the acquisition window in  
33 VASO experiments. In addition, it has been shown that the application of SMS-EPI can be  
34 advantageous to overcome brain coverage limitations in ASL (Feinberg et al., 2013;  
35 Ivanov et al., 2014; Kim et al., 2013b; Wang et al., 2015).

36 The purpose of this study is to implement and evaluate high-resolution functional  
37 imaging with VASO and BOLD contrast using SMS-EPI for concurrent imaging of CBV and  
38 oxygenation level.

1 This study focuses on the most important limitations of VASO-fMRI: the challenges to  
2 simultaneously acquire enough imaging slices to cover multiple brain areas, and to  
3 increase the slice resolution within an extended brain region. The novel VASO sequence  
4 is applied in three experimental setups: **A)** high-resolution acquisition of distant brain  
5 areas in the visuo-motor network (V1/V5/M1/S1); **B)** high-resolution acquisition of an  
6 imaging slab covering the entire M1/S1 hand region; **C)** low-resolution acquisition with  
7 near to whole-brain coverage.

## 8 **2. Materials and Methods**

### 9 **2.1. MR sequence**

10 MRI data were acquired with ten healthy right-handed participants (age 22-29 years).  
11 All procedures were approved by the Ethics Committee of the University of Leipzig.  
12 Informed written consent was given by all volunteers. SMS-SS-SI VASO was  
13 implemented on a MAGNETOM 7T scanner (Siemens Healthcare, Erlangen, Germany)  
14 in IDEA. For RF transmission and reception, a single-channel-transmit/32-channel-  
15 receive head coil (Nova Medical, Wilmington, MA, USA) was used. Functional data  
16 were acquired using an SMS two-dimensional (2D) single-shot EPI readout. The timing  
17 of magnetization preparation and interleaved acquisition of VASO and BOLD data is  
18 schematically depicted in Fig. 1. Sequence parameters were:  $T_{11}/T_{12}/TR =$   
19  $1100/2600/3000$  ms, nominal excitation flip angle was  $\alpha = 70^\circ\text{-}90^\circ$  dependent on the  
20 head size and the corresponding variation of the transmit voltage within SAR limits,  
21 across all functional experiments. The summation of multi-band sinc-pulses was  
22 conducted with optimized phase schedules for minimizing peak RF power (Wong,  
23 2012). VASO can be contaminated by inflow of non-inverted, especially, when blood  $T_1$   
24 is not much shorter than TR (Donahue et al., 2006). Such inflow effects can be  
25 avoided, when the blood-nulling time is shorter than the time that blood needs to  
26 arrive from the arteries in the neck to the micro vessels of the imaging slice (Huber et  
27 al., 2014). Here, a  $T_{11} = 1100$  ms is chosen, which includes an additional leeway of 200  
28 ms compared to the estimated arterial arrival time in the sensorimotor cortex  
29 (Mildner et al., 2014). The blood nulling time was manipulated by means of an  
30 adjusted inversion efficiency of 87% in a  $B_1$ -independent manner by using a phase skip  
31 of the RF field during inversion as described in (Huber et al., 2014c). The inversion  
32 pulse shapes are based on the TR-FOCI pulse (Hurley et al., 2010). The efficiency of the  
33 pulse was 94% (measured in pilot experiments). This means that 6% of the  
34 magnetization is lost during the application of the pulse. The inversion pulse  
35 amplitude was adjusted to have a minimum of  $10\ \mu\text{T}$  down to the Circle of Willis  
36 across all participants by used a transmitter voltage of 340 V. The overall energy  
37 deposition of the sequence never exceeded  $2.1\ \text{W/kg}$ , according to the SAR estimation  
38 of the vendor. The blood nulling time is calculated based on the assumed value of

1 blood  $T_1 = 2100$  ms, following earlier VASO studies at 7 T (Huber et al., 2014a; Huber  
2 et al., 2015; Huber et al., 2014c).

3 With increasing field strength, the positive BOLD signal change during neural  
4 activation increasingly counteracts the negative VASO signal change. The GE-BOLD  
5 effect typically has two components: intra-vascular and extravascular. At 7 T, the  
6 extravascular BOLD dominates the intravascular BOLD by more than 90% (Donahue et  
7 al., 2010; Uludağ et al., 2009). This extravascular BOLD contamination is considerably  
8 larger than the desired VASO signal change and needs to be corrected for. In SS-SI  
9 VASO, an interleaved, pair-wise acquisition of VASO and BOLD images is used to  
10 distinguish between BOLD and VASO signal components of the resulting signal. When  
11 the pure BOLD contrast contribution is known, the BOLD-contamination in the VASO  
12 image can be factored out, as described earlier (Huber et al., 2014a). In short, both  
13 BOLD and VASO time series are expected to have the same BOLD  $T_2^*$ -weighting but  
14 different VASO  $T_1$  weighting. Hence, when the voxel-wise ratio image between the  
15 BOLD and the VASO images is formed, the  $T_2^*$ -weighting is canceled out. This provides  
16 a BOLD-corrected VASO contrast. As long as both images are acquired with the  
17 identical EPI module, the  $T_2^*$ -weighting cancels out, independent of TE and readout  
18 duration. This BOLD correction mechanism relies on the assumption that changes in  
19 BOLD weighting are slower than the time between consecutive image acquisitions (3 s  
20 for a pair of VASO and BOLD). This means that any temporal dynamics of the BOLD signal  
21 change faster than 3 s will not be corrected for. Furthermore, it assumes that  
22 extravascular effects contribute much more to the BOLD response than intravascular  
23 effects. In this correction scheme, BOLD contaminations are considered to be solely  
24 based on changes in  $T_2^*$ . Hence, the applied correction scheme is assumed to account  
25 for BOLD contaminations in all compartments of the vascular tree including arteries,  
26 capillaries and veins inside and outside the GM tissue. This means that the BOLD-  
27 correction is not expected to have any limitations with respect to spatial resolution.

28 All functional experiments consisted of one-minute blocks repeated 12 times. The  
29 VASO sequence parameters concerning resolution, acceleration and position were  
30 optimized for three specific cases described as follows:

### 31 **2.1.1. Experiment A: Two high-resolution slice groups**

32 Two slice groups were positioned to cover V1/V5 and M1/S1 in 6 out of the 10  
33 participants, using the following sequence parameters: nominal resolution =  
34  $0.97 \times 0.97 \times 1.1 \text{ mm}^3 - 1 \times 1 \times 1.5 \text{ mm}^3$ , depending on the participant's brain  
35 anatomy; no slice gaps;  $2 \times 5 = 10$  slices; SMS factor = 2; field-of-view (FoV) shift  
36 (CAIPI factor) = 1; GRAPPA factor = 3, segmented reference line acquisition;  $TE$   
37 = 34 ms. The maximal time difference of image acquisition to the blood nulling  
38 time  $\Delta T_I$  was 162 ms. This means that the first excitation pulse was applied 162

ms before the blood nulling time point and the last excitation pulse was applied 162 ms after the blood nulling time point as indicated in Fig. 1. The distance between the centers of the two slice groups was 14 – 17 mm, depending on tilting angle and the participants' anatomy. This distance refers to the gap between the two yellow imaging slabs depicted in Fig. 2A. Partial Fourier imaging was kept minimal with a factor of = 7/8. The fat saturation pulse flip angle was set to 30°, assuming that most of the fat signal due to its short  $T_2$  would be decayed during the EPI readout anyway, not leading to serious fat artifacts. The functional paradigm consisted of three conditions: 20s rest, 20s visual task with a high-contrast static star field, and 20 s visual task with a high-contrast moving star field as in (Huk et al., 2002) with concurrent finger motion during the star motion. The finger motion consisted of pinch-like movement and touch of index finger, middle finger, ring finger, and little finger (consecutively) towards and away from the thumb with a self-paced frequency of approximately 0.25 – 0.75 Hz.

#### 2.1.2. Experiment B: Whole M1 coverage with high spatial resolution

One slice group was positioned to cover the entire areas of M1/S1 in 6 out of the 10 participants, with the following sequence parameters: nominal resolution =  $1 \times 1 \times 1.2 \text{ mm}^3$  –  $1 \times 1 \times 1.5 \text{ mm}^3$ , depending on the participant's brain anatomy; 50% – 70% slice gap; 15 slices; maximal  $\Delta T/1$  = 175 ms; SMS factor = 3; FoV shift = 1/3; GRAPPA factor = 2 with FLEET (Chapman et al., 1987) reference lines (Polimeni et al., 2015);  $TE$  = 33 ms. To minimize  $T_2^*$ -blurring, partial Fourier imaging was not used (Huber et al., 2014b). The functional paradigm consisted of unilateral finger-tapping (alternating 30-s rest vs. 30-s tapping). The tapping task was identical to experiment A.

#### 2.1.3. Experiment C: Near whole-brain coverage with low spatial resolution

20 slices were positioned to cover the brain in 6 out of the 10 participants with the sequence parameters: nominal resolution =  $3 \times 3 \times 3 \text{ mm}^3$ ; 50% slice gaps; maximal,  $\Delta T/1$  = 75 ms; SMS factor = 4; FoV shift factor = 1/3; GRAPPA factor = 2 with FLEET reference lines;  $TE$  = 14 ms, partial Fourier factor = 7/8. The functional paradigm was identical to that of experiment A.

#### 2.1.4. Direct comparison of SMS-VASO with non-SMS-VASO

In order to evaluate, whether the application of SMS imaging in VASO may degrade the image quality, direct comparisons of SMS-VASO and non-SMS-VASO were conducted. In three additional participants, the imaging protocols described above (experiments A-C) were repeated without functional stimulation along with a variant with SMS factor 1 (non-SMS) leaving all other parameters the same. With the reduced acceleration in the non-SMS-VASO

1 case, only 20% to 50% of the imaging region could be covered compared to  
2 SMS-VASO. Hence, not all ROIs could be compared (V1, V5, M1/S1). Here, the  
3 sensory motor area was chosen as a region for comparison. I.e. the imaging  
4 slices were positioned to cover the M1/S1 area with both protocols, with the  
5 SMS-VASO and the non-SMS-VASO.

6 Note that experiment A uses the segmented GRAPPA reference line acquisition, while  
7 experiment B and C use FLEET GRAPPA reference line acquisition. The GRAPPA  
8 reference line acquisition scheme of choice was decided based on respective  
9 susceptibility to  $B_0$ -inhomogenities, appearance of GRAPPA-ghosts and tSNR  
10 obtained in respective pilot experiments.

## 11 **2.2. Image reconstruction**

12 Image reconstruction was performed online on the scanner. The data with 7/8 partial  
13 Fourier were zero-filled. Signals from the simultaneously acquired slices were first un-  
14 aliased with an implementation of SplitSlice-GRAPPA with LeakBlock (Cauley et al.,  
15 2014) and a 3x3 kernel, as distributed with the MGH blipCAIPI C2P (Setsompop et al.,  
16 2012b)(<http://www.nmr.mgh.harvard.edu/software/c2p/sms>); this was followed by  
17 the vendor's in-plane GRAPPA reconstruction (Griswold et al., 2002), using a 2x3  
18 kernel. Finally, the complex coil images were combined using the vendor's  
19 implementation of adaptive combine.

## 20 **2.3. Data analysis**

21 All MR images were motion corrected using SPM8 (Wellcome Department, University  
22 College London, UK). Statistical analysis was done using FSL FEAT (Version 5.98)  
23 (Worsley, 2001). One of the major goals of this study is to investigate the spatial  
24 features of CBV and BOLD signal changes in brain areas that are already known to be  
25 involved in the functional task. Therefore, the purpose of the statistical analysis is not  
26 to isolate significantly activated areas from other brain areas, but to investigate the  
27 range of Z-values within the ROIs. Hence, Z-value thresholds in statistical activation  
28 maps are kept relatively low, minimizing false negative voxels despite increasing the  
29 risk of false positive voxels. Statistical data were not thresholded by cluster size. In  
30 order to estimate and eliminate BOLD contamination in the CBV-weighted data, the  
31 VASO signal was corrected using the BOLD signal acquired interleaved, as in previous  
32 studies (Huber et al., 2014c). In the evaluation of data from experiment B (thick high-  
33 resolution imaging slab covering M1), missing signal from inter-slice gaps was linearly  
34 extrapolated from adjacent slices to provide undistorted signal maps in the coronal  
35 and sagittal orientations. No spatial smoothing was applied during any part of the  
36 offline data analysis.  
37

## 38 **3. Results**



### 3.1. Experiment A: Two slice groups covering V1, V5, M1, and S1

The results of SMS-VASO imaging of the visuo-motor network are depicted in Fig. 2. Maps of temporal SNR (tSNR) are depicted in Fig. 2A for one representative subject. It can be seen that the proposed method has enough tSNR to significantly detect strong activity changes in V1 and in the contralateral sensory motor cortex. The inter-subject average tSNR of the VASO and BOLD signal in grey matter (GM) ROIs is  $16 \pm 3$  and  $22 \pm 4$ , respectively. Indications of positive and negative activity changes in the ipsilateral sensory-motor region and in V5 are clearly visible, but not as robustly as in the contralateral sensory-motor region.

The contralateral M1 and S1 yielded significant signal increases during the unilateral finger motion task. The ipsilateral M1 shows a positive BOLD signal change and CBV increase, while ipsilateral S1 shows a negative BOLD and CBV decrease in all participants.

Black arrows in the lower slice of the results in Fig. 2A refer to fat signal artifacts, which most probably result from insufficient fat suppression. Since they are expected to be the same at every time point during the experiment, they can be considered negligible with respect to the functional results presented.

Fig. 2B depicts the reproducibility and stability of the results across participants. The average signal changes of the contralateral BOLD and VASO responses were  $(2.3 \pm 0.5)\%$  and  $(-1.7 \pm 0.5)$  ml/100ml respectively in M1 and  $(2.9 \pm 0.4)\%$  and  $(2.0 \pm 0.5)$  ml/100ml in S1, respectively. The average signal changes of the ipsilateral BOLD and VASO responses were  $(1.8 \pm 0.5)\%$  and  $(-1.1 \pm 0.4)$  ml/100ml, respectively in M1 and  $(-1.6 \pm 0.4)\%$  and  $(1.2 \pm 0.4)$  ml/100ml in S1, respectively.

It is worth pointing out that BOLD is inherently sensitive to task-correlated motion (Fig. 2; green arrows in participants 1 and 2) (Schulz et al., 2014), while any variations in the signal beyond functional  $T_1$  changes are inherently suppressed in the BOLD-correction procedure (which involves taking the ratio of sequential images) in SS-SI VASO.

The average time courses of GE-BOLD and VASO response signals are depicted in Fig. 2C. V1 is sensitive to contrast changes, and is largely independent of the amount of motion in the visual presentation. V5, contralateral M1, contralateral S1, and ipsilateral M1 have an overall activation response during movements, while ipsilateral S1 has an overall deactivation response during unilateral movements. This is consistent with CBV and BOLD signal responses in previous studies (Huber et al., 2015). Following the BOLD and VASO time courses, it can be seen that there is no significant post-stimulus undershoot, even in V1. This is consistent with previous BOLD and VASO results using the same visual moving star field paradigm (Huber et al., 2014c), which shows a slightly different response shape compared to a more common

1 flickering checkerboard paradigm. It must be also noted that the occurrence of a  
2 significant post-stimulus undershoot is highly dependent on the extent of the area of  
3 interest (van Zijl, et al., 2012), and the inter-stimulus resting period used (Huber et al.,  
4 2014d).

### 5 **3.2. Experiment B: High-resolution M1 coverage**

6 The results of SMS-VASO for high-slice-resolution imaging of an imaging slab spanning  
7 across M1 are depicted in Fig. 3. The average tSNR (Fig. 3A) of VASO and BOLD signal  
8 in GM ROIs of M1/S1 is  $14 \pm 2$  and  $24 \pm 4$ , respectively. The tSNR is sufficient to obtain  
9 highly consistent and reproducible results across participants (Fig. 3B). The activity  
10 pattern in contralateral and ipsilateral sensory motor cortex is very similar to the  
11 results from experiment A (Fig. 2).

## 1       **Experiment C: Near whole-brain coverage acquisition**

2       The results of SMS-VASO for low-resolution acquisitions to cover nearly the entire  
3       brain are depicted in Fig. 4. Average tSNR (Fig. 4A) of VASO and BOLD signal in GM  
4       ROIs is  $33 \pm 6$  and  $57 \pm 12$ , respectively. The activity patterns are very similar across  
5       participants (Fig. 4B), and they are consistent with the results of experiment A (Fig. 2).  
6       The limited robustness in the detection of small negative response in ipsilateral S1 and  
7       the small positive response in V5 might be a result of the partial voluming of GM with  
8       white matter and cerebro-spinal fluid (CSF), or partial voluming of opposite responses  
9       in M1/S1 at low resolution.

### 10       **3.3. Direct comparison of SMS-VASO with non-SMS-VASO**

11       The results of the direct comparison of SMS-VASO and non-SMS-VASO are depicted in  
12       Fig. 5. The depicted tSNR maps show that there is no significant image quality  
13       reduction, when applying SMS-VASO compared to non-SMS-VASO. The tSNR in the  
14       M1/S1 region for SMS-VASO and non-SMS VASO was  $18 \pm 4$  and  $19 \pm 4$  for experiment  
15       A,  $15 \pm 3$  and  $14 \pm 4$  for experiment B, and  $33 \pm 5$  and  $29 \pm 4$  for experiment C,  
16       respectively. The negligible tSNR difference with and without SMS imaging is  
17       consistent with previous studies. Setsompop et al. showed that the g-factor remains  
18       around 1.0 for SMS imaging with CAIPI and SMS factors up to 3 (Setsompop, et al.,  
19       2012).

### 20       **3.4. Summary of statistical numerical results of functional results**

21       The statistical Z-values within activated regions depicted in Figs 2-4 are summarized in  
22       Tab. 1. The manually selected ROIs are V1, V5, and the contralateral side of M1. It can  
23       be seen that the statistical Z-values are larger for BOLD compared to VASO. This is  
24       consistent with the higher tSNR in BOLD compared to VASO.

## 25       **4. Discussion**

26       The results shown in Figs. 2 and 3 clearly demonstrate a major advantage of high-resolution  
27       VASO. This methodology can distinguish different individual responses in neighboring but  
28       distinct brain areas (e.g. ipsilateral S1 and M1), that cannot be separated with GE-BOLD,  
29       with low-resolution fMRI, or when applying spatial smoothing (Stelzer et al., 2014).

### 30       **4.1. Other 3D imaging approaches**

31       Besides the combination of VASO with SMS acquisition, several advanced imaging  
32       strategies have been proposed to increase the coverage of VASO (Lu et al., 2013).  
33       These include MAGIC VASO (Lu et al., 2004), 3D GRASE VASO (Donahue et al., 2009;  
34       Poser and Norris, 2009), HASTE VASO (Poser and Norris, 2007), multi-shot 3D turbo  
35       field echo VASO (Hua et al., 2013), and multi-shot 3D TSE VASO (Cretti et al., 2013).  
36       Compared with these previously suggested approaches for increasing the VASO

1 coverage, the proposed SMS acquisition is particularly beneficial for obtaining high  
2 spatial resolution, because it can increase the coverage without increasing the  
3 acquisition duration. For a further increase in SMS-VASO coverage, the technique  
4 could be combined with the MAGIC VASO (Lu et al., 2004) approach, in which the  
5 blood signal is forced to pass through zero multiple times by means of additional  
6 inversion pulses during the acquisition. However, the SAR constraints of the  
7 corresponding additional inversion pulses at high field strengths might limit its  
8 application dependent on the efficiency of the hardware available. More research is  
9 needed to determine the applicability of MAGIC VASO at high field strengths.

#### 10 **4.2. Limitation by TR for vasculature refilling**

11 The proposed high tSNR of SS-SI VASO compared to the traditional VASO approach is  
12 based on additional assumptions regarding the blood flow dynamics. For complete  
13 nulling of once-inverted blood magnetization in SS-SI VASO, it is required that all the  
14 blood within the imaging slice is refilled within one TR. It is estimated in the original  
15 SS-SI VASO paper (Huber et al., 2014c) that it takes 1-1.5 s until the microvasculature  
16 of a single slice is refilled with fresh blood. For a thicker imaging slab, the refilling time  
17 is expected to be correspondingly longer. In order to avoid incomplete blood nulling in  
18 the proposed SMS-SS-SI VASO method, we chose the TR to be minimally 3 s, giving the  
19 blood enough time to refill the entire brain. With this sequence timing, the measured  
20 changes in V1 are not different from the estimated changes in V1 in previous studies,  
21 acquired with the same activation task but a single-slice implementation (Huber et al.,  
22 2014c). This suggests that with the sequence timing used in this study, the acquisition  
23 of more slices does not lead to additional violation of the refill condition.

#### 24 **4.3. Effect of incomplete blood nulling**

25 There are two major sources of incomplete blood nulling in VASO. (i) Uncertainties in  
26 blood  $T_1$ , e.g. due to physiologic reasons, such as oxygenation level and inter-subject  
27 variations in hematocrit. (ii) Variations in  $TR$ , due to technical reasons, e.g. the  
28 consecutive acquisition of multiple 2D slices. It has been recently shown that the  
29 difference between arterial blood  $T_1$  and venous blood  $T_1$ , and the influence of  
30 moderate variations in hematocrit lies in the range of 100 – 200 ms (Grgac et al., 2012;  
31 Rane and Gore, 2013). A sequence of up to five consecutive excitation pulses causes a  
32 variation in blood-nulling time of the same order (75 – 175 ms). The corresponding  
33 incomplete blood nulling can result in an error in the VASO signal change of up to 14%  
34 relative to the total VASO signal change. This means that in the worst-case scenario,  
35 the measured CBV change of  $2.0 \pm 0.5$  ml/100ml in contralateral M1 might have an  
36 additional source of uncertainty, to become  $2.0 \pm 0.5$  (inter-subject standard  
37 deviation)  $\pm 0.28$  (uncertainty in blood-nulling time) ml/100ml. Since the  
38 corresponding bias of VASO quantification from slices acquired before blood nulling  
39 and from slices acquired after blood nulling is opposite in sign, these biases are

1 believed to largely cancel each other out after averaging across ROIs and, thus, to  
2 have no significant effect on the averaged results of this study.

#### 3 **4.4. Signal change at cortical surface**

4 The VASO contrast at the cortical surface can suffer from artifacts arising from (i)  
5 BOLD contaminations and (ii) dynamic changes in CSF volume (Lu et al., 2013) that  
6 could complicate the interpretation of CBV changes at the cortical surface. While  
7 conventional VASO contrast generation can suffer from these contaminations, they  
8 have only a limited effect in the application of SS-SI VASO, as discussed in (Huber et  
9 al., 2015). (i) Any extravascular BOLD contamination is corrected for in SS-SI VASO by  
10 means of dynamic division by the interleaved-acquired BOLD signal. (ii) Contamination  
11 of dynamic changes in partial volume from CSF can be minimized in SS-SI VASO by  
12 manipulation of the steady-state CSF magnetization such that it has a positive phase  
13 and a similar signal compared to GM. Hence, it is expected that the high GM tissue  
14 specificity of SS-SI VASO is dominated by the sensitivity to microvascular vessels.

15 In two out of six participants, there are a few voxels clearly between the two sides of  
16 the contralateral sulcus that show a positive VASO response, suggesting  
17 vasoconstriction (participant 2 and 4 in Fig. 3). Such features have also been reported  
18 by others, and have been interpreted as volume constriction of large draining veins  
19 (Blockley et al., 2012) or neural inhibition (Trampel et al., 2013).

#### 20 **4.5. Functional specificity**

21 Data given in Figs. 2 and 3 show that VASO fMRI can better delineate individual GM  
22 territories, as compared with GE-BOLD which invariably shows largest activity  
23 between the opposing GM banks of a sulcus. The higher spatial specificity of VASO to  
24 GM tissue without contamination from independent of large draining veins can be  
25 particularly rewarding when opposing GM banks of a sulcus comprise different nodes  
26 of a brain network (e.g. M1 and S1). Where there is positive response in opposite GM  
27 areas (e.g. contralateral M1/S1), the GE-BOLD signal of both areas is amplified by the  
28 draining vein effect (Turner, 2002) to be maximal in larger veins above the cortical  
29 surface (see purple inserts in Figs. 2 and 3).

30 In the case of positive and negative responses in opposing GM banks (e.g. ipsilateral  
31 M1/S1), the mixing of deoxyhemoglobin changes arising from opposite responses on  
32 opposite sides of the sulcus can result in an attenuated GE-BOLD signal (see blue  
33 inserts in Figs. 2 and 3). For example, pial veins within the sulcus can drain both M1  
34 and S1, and hence their BOLD signal might reflect a mixture of activity in both areas.  
35 Such features, which have not previously been discussed in the literature, can make it  
36 difficult to interpret the corresponding BOLD signal from opposite sides of the sulcus.  
37 The higher specificity to brain tissue in VASO, avoids such limitations, and depicts  
38 responses in opposing GM banks of the central sulcus independently.

#### 1 **4.6. Response in the ipsilateral hemisphere**

2 Figs. 2 and 3 show that unilateral finger movement evokes a positive response in  
3 ipsilateral M1, but a negative response in ipsilateral S1. This particular result has been  
4 found to be highly dependent on stimulus paradigm and strength. While low force  
5 (usually 5% of individual maximal voluntary contraction) has been shown to evoke a  
6 negative BOLD response, and reductions in blood flow and metabolism in ipsilateral  
7 sensori-motor ROIs, positive responses in ipsilateral M1 have been observed when  
8 stronger forces and more demanding tasks are used (Dettmers et al., 1995).

#### 9 **4.7. Magnetization transfer effects in SMS-VASO**

10 The application of off-resonant RF pulses in inversion recovery sequences such as  
11 VASO, results in magnetization transfer (MT) effects. These MT effects can result in an  
12 accelerated longitudinal relaxation mimicking a different  $T_1$ . In the application of SMS-  
13 VASO the (off-) resonant excitation pulses have increased RF amplitude and thus also  
14 higher potential to induce MT effects. While there are significant MT effects in most  
15 brain tissues, it has been shown that blood exhibits a very small MT effect due to its  
16 low concentration of macromolecules (Wolff and Balaban, 1989; Balaban et al., 1991).  
17 This means that while off-resonant RF pulses affect the tissue relaxation, blood  
18 relaxation is not altered, leaving the blood nulling time unaffected. In fact, this unique  
19 difference between blood and brain tissue regarding MT effects has been used to  
20 actively enhance SNR in high field VASO experiments by means of additional high-  
21 power MT pulses (Hua et al., 2009 and 2013). In conclusion, the additional MT effects  
22 due to the multiband excitation pulses do not alter the blood nulling time and CBV  
23 quantification, but are believed to result in a slightly larger GM signal and  
24 corresponding SNR increase.

#### 25 **4.8. Extensibility to lower field strengths**

26 While all experiments in this study were conducted at 7 T, its application might be  
27 advantageous at 3 T as well. The shorter blood  $T_1$  at lower field strengths (Zhang et al.,  
28 2013), however, results in reduced signal gain applying SS-SI VASO as opposed to the  
29 original VASO (Huber et al., 2014c). Additionally, the larger relative thermal noise  
30 contribution at 3 T compared to 7 T can also be an additional constraint in going to  
31 such high spatial resolutions at lower field strengths. The low-resolution approach of  
32 experiment C, however, might be a useful tool for quantitative fMRI techniques, such  
33 as calibrated BOLD, both at 3 T and 7 T. More research is necessary to evaluate the  
34 combination of VASO and SMS imaging at 3 T.

#### 35 **4.9. Other imaging modalities**

36 Spin echo (SE) BOLD fMRI has been suggested to have higher specificity to the  
37 microvasculature (Uludağ et al., 2009) and its utility for laminar and columnar fMRI

1 has been demonstrated in animals (Goense et al., 2012; Harel et al., 2006; Zhao et al.,  
2 2006) and in humans (Yacoub et al., 2005; Yacoub et al., 2008). However, it suffers  
3 from much lower sensitivity, especially at high resolution (Yacoub et al., 2005), which  
4 may limit the widespread application of the technique (Boyacioglu et al., 2014; Budde  
5 et al., 2014; Harmer et al., 2012).

## 7 5. Conclusion

8 SMS-EPI has a major advantage in VASO fMRI by acquisition of more slices during the  
9 short time period  $\Delta T_I$  when blood magnetization is sufficiently nulled. Due to the  
10 increased brain coverage and better localization specificity of VASO to GM tissue  
11 compared to GE-BOLD signal, the proposed method can play an important role in high-  
12 resolution fMRI at 7 T.

## 13 6. Acknowledgements

14 We thank Domenica Wilfling and Elisabeth Wladimirow for radiographic assistance.  
15 We thank Steve Cauley at MGH for sharing the interface of their image reconstruction  
16 for use with our SMS-VASO sequence. The research was supported by the Max Planck  
17 Society and Netherlands Organization for Scientific Research NWO: VIDI 452-11-002 to  
18 Kamil Uludağ. Maria Guidi was supported by the Initial Training Network, HiMR,  
19 funded by the FP7 Marie Curie Actions of the European Commission (FP7-PEOPLE-  
20 2012-ITN-316716). Preliminary accounts of this work have been presented in the  
21 Proceedings of the 23th Annual Meeting of ISMRM, Toronto, Canada, 2015 (abstract  
22 600).

## 23 7. References

- 24 Balaban R.S., Chesnick S., Hedges K., Samaha F., Heineman F.W. Magnetization transfer contrast in MR  
25 imaging of the heart. *Radiology* 1991; 180:671–675.
- 26 Bandettini, P.A., 2012. Twenty years of functional MRI: the science and the stories. *Neuroimage* 62,  
27 575-588.
- 28 Blockley, N.P., Driver, I.D., Fisher, J.A., Francis, S.T., Gowland, P.A., 2012. Measuring venous blood  
29 volume changes during activation using hyperoxia. *Neuroimage* 59, 3266-3274.
- 30 Boyacioglu, R., Schulz, J., Muller, N.C., Koopmans, P.J., Barth, M., Norris, D.G., 2014. Whole brain, high  
31 resolution multiband spin-echo EPI fMRI at 7 T: A comparison with gradient-echo EPI using a  
32 color-word Stroop task. *Neuroimage* 97, 142–150.
- 33 Budde, J., Shajan, G., Zaitsev, M., Scheffler, K., Pohmann, R., 2014. Functional MRI in human subjects  
34 with gradient-echo and spin-echo EPI at 9.4T. *Magn. Reson. Med.* 71, 209–218.
- 35 Cauley, S.F., Polimeni, J.R., Bhat, H., Wald, L.L., Setsompop, K., 2014. Interslice leakage artifact  
36 reduction technique for simultaneous multislice acquisitions. *Magn Reson Med* 72, 93-102.
- 37 Chapman, B., Turner, R., Ordidge, R.J., Doyle, M., Cawley, M., Coxon, R., Glover, P., Mansfield, P.,  
38 1987. Real-time movie imaging from a single cardiac cycle by NMR. *Magn Reson Med* 5, 246-  
39 254.

- 1 Cretti, F.R., Summers, P.E., Porro, C.A., 2013. Multi-shot turbo spin-echo for 3D vascular space  
2 occupancy imaging. *Magn Reson Imaging* 31, 875-881.
- 3 Dettmers, C., Fink, G.R., Lemon, R.N., Stephan, K.M., Passingham, R.E., Silbersweig, D., Holmes, A.,  
4 Ridding, M.C., Brooks, D.J., Frackowiak, R.S., 1995. Relation between cerebral activity and  
5 force in the motor areas of the human brain. *J Neurophysiol* 74, 802-815.
- 6 Donahue, M.J., Hoogduin, H., van Zijl, P.C.M., Jezzard, P., Luijten, P.R., Hendrikse, J., 2010 Blood  
7 oxygenation level-dependent (BOLD) total and extravascular signal changes and  $\Delta R2^*$  in  
8 human visual cortex at 1.5, 3.0 and 7.0 T. *NMR Biomed* 24, 25-34.
- 9 Donahue, M.J., Blicher, J.U., Ostergaard, L., Feinberg, D.A., MacIntosh, B.J., Miller, K.L., Gunther, M.,  
10 Jezzard, P., 2009. Cerebral blood flow, blood volume, and oxygen metabolism dynamics in  
11 human visual and motor cortex as measured by whole-brain multi-modal magnetic resonance  
12 imaging. *J Cereb Blood Flow Metab* 29, 1856-1866.
- 13 Donahue, M.J., Lu, H., Jones, C.K., Edden, R.A., Pekar, J.J., van Zijl, P.C., 2006. Theoretical and  
14 experimental investigation of the VASO contrast mechanism. *Magn Reson Med* 56, 1261-  
15 1273.
- 16 Feinberg, D.A., Beckett, A., Chen, L., 2013. Arterial spin labeling with simultaneous multi-slice echo  
17 planar imaging. *Magn Reson Med* 70, 1500-1506.
- 18 Feinberg, D.A., Moeller, S., Smith, S.M., Auerbach, E., Ramanna, S., Gunther, M., Glasser, M.F., Miller,  
19 K.L., Ugurbil, K., Yacoub, E., 2010. Multiplexed echo planar imaging for sub-second whole  
20 brain fMRI and fast diffusion imaging. *PLoS One* 5, e15710.
- 21 Goense, J., Merkle, H., Logothetis, N.K., 2012. High-resolution fMRI reveals laminar differ-  
22 ences in neurovascular coupling between positive and negative BOLD responses. *Neuron* 76, 629-639.
- 23 Grgac, K., van Zijl, P.C., Qin, Q., 2012. Hematocrit and oxygenation dependence of blood (1) H(2) O  
24 T(1) at 7 tesla. *Magn Reson Med* 70, 1153-1159.
- 25 Griswold, M.A., Jakob, P.M., Heidemann, R.M., Nittka, M., Jellus, V., Wang, J., Kiefer, B., Haase, A.,  
26 2002. Generalized autocalibrating partially parallel acquisitions (GRAPPA). *Magn Reson Med*  
27 47, 1202-1210.
- 28 Harel, N., Lin, J., Moeller, S., Ugurbil, K., Yacoub, E., 2006. Combined imaging-histological study of  
29 cortical laminar specificity of fMRI signals. *Neuroimage* 29, 879-887.
- 30 Harmer, J., Sanchez-Panchuelo, R.M., Bowtell, R., Francis, S.T., 2012. Spatial location and strength of  
31 BOLD activation in high-spatial-resolution fMRI of the motor cortex: a comparison of spin echo  
32 and gradient echo fMRI at 7 T. *NMR Biomed.* 25, 717-725.
- 33 Hua J., Donahue M.J., Zhao J.M., Grgac K., Huang A.J., Zhou J., van Zijl P.C. Magnetization transfer  
34 enhanced vascular-space-occupancy (MT-VASO) functional MRI. *Magn Reson Med*  
35 2009;61:944.
- 36 Hua, J., Jones, C.K., Qin, Q., van Zijl, P.C., 2013. Implementation of vascular-space-occupancy MRI at  
37 7T. *Magn Reson Med* 69, 1003-1013.
- 38 Huber, L., Goense, J., Kennerley, A.J., Ivanov, D., Krieger, S.N., Lepsien, J., Trampel, R., Turner, R.,  
39 Moller, H.E., 2014a. Investigation of the neurovascular coupling in positive and negative BOLD  
40 responses in human brain at 7 T. *Neuroimage* 97, 349-362.
- 41 Huber, L., Goense, J., Kennerley, A.J., Trampel, R., Guidi, M., Reimer, E., Ivanov, D., Neef, N., Gauthier,  
42 C.J., Turner, R., Moller, H.E., 2015. Cortical lamina-dependent blood volume changes in human  
43 brain at 7 T. *Neuroimage* 107, 23-33.
- 44 Huber, L., Guidi, M., Goense, J., Mildner, T., Trampel, R., Schulz, J., Eichner, C., Turner, R., Möller, H.E.,  
45 2014b. The magnitude point spread function is an inadequate measure of T2\*-blurring in EPI.  
46 *Proceedings of the International Society of Magnetic Resonance in Medicine* 23, 2056.
- 47 Huber, L., Ivanov, D., Krieger, S.N., Streicher, M.N., Mildner, T., Poser, B.A., Moller, H.E., Turner, R.,  
48 2014c. Slab-selective, BOLD-corrected VASO at 7 Tesla provides measures of cerebral blood  
49 volume reactivity with high signal-to-noise ratio. *Magn Reson Med* 72, 137-148.



1 Huber, L., Kennerley, A.J., Ivanov, D., Gauthier, G.J., Moeller, H.E., Turner, R., 2014c, Trial-wise  
2 investigation of cerebral blood volume change in human brain at 7T, Proceedings of the  
3 International Society of Magnetic Resonance in Medicine 22, 3095.

4 Hurley, A.C., Al-Radaideh, A., Bai, L., Aickelin, U., Coxon, R., Glover, P., Gowland, P.A. Tailored RF pulse  
5 for magnetization inversion at ultrahigh field. Magn Reson Med. 63, 51-58

6 Huk, A.C., Dougherty, R.F., Heeger, D.J., 2002. Retinotopy and functional subdivision of human areas  
7 MT and MST. J. Neurosci. 22, 7195-7205.

8 Ivanov, D., Poser, B.A., Huber, L., Pfeuffer, J., Uludag, K., 2014. Whole-brain perfusion measurements  
9 at 7T using pulsed arterial spin labelling and simultaneous multi-slice multi-echo echo planar  
10 imaging. Proceedings of the International Society of Magnetic Resonance in Medicine 22,  
11 2698.

12 Kim, S.G., Harel, N., Jin, T., Kim, T., Lee, P., Zhao, F., 2013a. Cerebral blood volume MRI with  
13 intravascular superparamagnetic iron oxide nanoparticles. NMR Biomed 26, 949-962.

14 Kim, T., Shin, W., Zhao, T., Beall, E.B., Lowe, M.J., Bae, K.T., 2013b. Whole brain perfusion  
15 measurements using arterial spin labeling with multiband acquisition. Magn Reson Med 70,  
16 1653-1661.

17 Lu, H., Donahue, M.J., Jones, C.K., van Zijl, P.C., 2005. Spatial characteristics of VASO fMRI at ultra-high  
18 resolution. Proceedings of the International Society of Magnetic Resonance in Medicine 22,  
19 0027.

20 Lu, H., Golay, X., Pekar, J.J., van Zijl, P.C.M., 2003. Functional magnetic resonance imaging based on  
21 changes in vascular space occupancy. Magn Reson Med 50, 263-274.

22 Lu, H., Hua, J., van Zijl, P.C., 2013. Noninvasive functional imaging of cerebral blood volume with  
23 vascular-space-occupancy (VASO) MRI. NMR Biomed 26, 932-948.

24 Lu, H., van Zijl, P.C., Hendrikse, J., Golay, X., 2004. Multiple acquisitions with global inversion cycling  
25 (MAGIC): A multislice technique for vascular-space-occupancy dependent fMRI. Magn Reson  
26 Med 51, 9-15.

27 Mildner, T., Muller, K., Hetzer, S., Trampel, R., Driesel, W., Moller, H.E., 2014. Mapping of arterial  
28 transit time by intravascular signal selection. NMR Biomed 27, 594-609.

29 Moeller, S., Yacoub, E., Olman, C.A., Auerbach, E., Strupp, J., Harel, N., Ugurbil, K., 2010. Multiband  
30 multislice GE-EPI at 7 tesla, with 16-fold acceleration using partial parallel imaging with  
31 application to high spatial and temporal whole-brain fMRI. Magn Reson Med 63, 1144-1153.

32 Polimeni, J.R., Bhat, H., Witzel, T., Benner, T., Feiweier, T., Inati, S.J., Renvall, V., Heberlein, K., Wald,  
33 L.L., 2015. Reducing sensitivity losses due to respiration and motion in accelerated echo  
34 planar imaging by reordering the autocalibration data acquisition. Magn Reson Med.

35 Poser, B.A., Norris, D.G., 2007. Measurement of activation-related changes in cerebral blood volume:  
36 VASO with single-shot HASTE acquisition. Magn Reson Mater Phy 20, 63-67.

37 Poser, B.A., Norris, D.G., 2009. 3D single-shot VASO using a Maxwell gradient compensated GRASE  
38 sequence. Magn Reson Med 62, 255-262.

39 Rane, S.D., Gore, J.C., 2013. Measurement of T1 of human arterial and venous blood at 7T. Magn  
40 Reson Imaging 31, 477-479.

41 Schulz, J., Siegert, T., Bazin, P.L., Maclaren, J., Herbst, M., Zaitsev, M., Turner, R., 2014. Prospective  
42 slice-by-slice motion correction reduces false positive activations in fMRI with task-correlated  
43 motion. Neuroimage 84, 124-132.

44 Scouten, A., Constable, R.T., 2007. Application and limitations of whole-brain MAGIC VASO functional  
45 fmaging. Magn Reson Med 58, 306-315.

46 Setsompop, K., Gagoski, B.A., Polimeni, J.R., Witzel, T., Wedeen, V.J., Wald, L.L., 2012a. Blipped-  
47 controlled aliasing in parallel imaging for simultaneous multislice echo planar imaging with  
48 reduced g-factor penalty. Magn Reson Med 67, 1210-1224.

49 Setsompop, K., Gagoski, B.A., Polimeni, J.R., Witzel, T., Wedeen, V.J., Wald, L.L., 2012b. Blipped-  
50 controlled aliasing in parallel imaging for simultaneous multislice echo planar imaging with  
51 reduced g-factor penalty. Magn Reson Med 67, 1210-1224.

1 Stelzer, J., Lohmann, G., Mueller, K., Buschmann, T., Turner, R., 2014. Deficient approaches to human  
2 neuroimaging. *Front Hum Neurosci* 8, 462.

3 Trampel, R., Schäfer, A., Huber, L., Heidemann, R.M., Turner, R., 2013. Negative BOLD in  
4 somatosensory cortex during simple finger tapping. *Proceedings of the International Society of*  
5 *Magnetic Resonance in Medicine*, p. 2339.

6 Turner, R., 2002. How much cortex can a vein drain? Downstream milustion of activation-related  
7 cerebral blood oxygenation changes. *Neuroimage* 16, 1062-1067.

8 Uludağ, K., Muller-Bierl, B., Ugurbil, K., 2009. An integrative model for neuronal activity- induced  
9 signal changes for gradient and spin echo functional imaging. *Neuroimage* 48, 150–165.

10 van Zijl, P.C.M., Hua, J., Lu, H. 2012 The BOLD post-stimulus undershoot, one of the most debated  
11 issues in fMRI. *NeuroImage* 62, 1092-1102.

12 Wang, Y., Moeller, S., Li, X., Vu, A.T., Krasileva, K., Ugurbil, K., Yacoub, E., Wang, D.J., 2015.  
13 Simultaneous multi-slice Turbo-FLASH imaging with CAIPIRINHA for whole brain distortion-  
14 free pseudo-continuous arterial spin labeling at 3 and 7T. *Neuroimage* 113, 279-288.

15 Wolff S.D., Balaban R.S., Magnetization transfer contrast (MTC) and tissue water proton relaxation in  
16 vivo. *Magn Reson Med* 1989;10:135– 144.

17 Wong, E., 2012. Optimized phase schedules for minimizing peak RF power in simultaneous multi-slice  
18 RF excitation pulses. In *Proceedings of the 20th Annual Meeting of ISMRM*, Melbourne,  
19 Victoria, Australia, p. 2209.

20 Worsley, K.J., 2001. Statistical analysis of activation images. In P. Jezzard, P. M. Matthews, S. M. Smith  
21 (eds). *Functional MRI: An introduction to Methods*. Oxford University Press, Oxford, UK, pp.  
22 251.

23 Yacoub, E., Van DeMoortele, P.F., Shmuel, A., Ugurbil, K., 2005. Signal and noise character- istics of  
24 Hahn SE and GE BOLD fMRI at 7 T in humans. *Neuroimage* 24, 738–750.

25 Yacoub, E., Harel, N., Ugurbil, K., 2008. High-field fMRI unveils orientation columns in humans. *Proc.*  
26 *Natl. Acad. Sci. U. S. A.* 105, 10607–10612.

27 Zhang, X., Petersen, E.T., Ghariq, E., De Vis, J.B., Webb, A.G., Teeuwisse, W.M., Hendrikse, J., van Osch,  
28 M.J., 2012. In vivo blood T(1) measurements at 1.5 T, 3 T, and 7 T. *Magn Reson Med*.

29 Zhao, F., Wang, P., Hendrich, K., Ugurbil, K., Kim, S.G., 2006. Cortical layer-dependent BOLD and CBV  
30 responses measured by spin-echo and gradient-echo fMRI: insights into hemodynamic  
31 regulation. *Neuroimage* 30, 1149–1160.

32

33 **Tables:**

34 Tab. 1: Statistical Z-value results of functional experiments.

VASO	Experiment A		Experiment B		Experiment C	
	Mean	STD	Mean	STD	Mean	STD
V1 area	4.6	1.3	ROI not in FOV		6.7	1.2
MT area	3.7	1.2	ROI not in FOV		4.6	1.1
M1 area (contralateral)	3.7	0.5	5.5	2.2	8.0	3.2

35

BOLD	Experiment A		Experiment B		Experiment C	
	Mean	STD	Mean	STD	Mean	STD
V1 area	7.7	1.2	ROI not in FOV		9.5	1.3
MT area	4.5	1.8	ROI not in FOV		6.3	0.7
M1 area (contralateral)	7.2	1.4	9.7	2.3	10.5	3.1

36

1

2 **Figure captions:**

3 **Fig. 1: Magnetization preparation, readout, and sequence timing.**

4 Schematic depiction of one TR in the SMS-VASO sequence starting with the application of an  
5 adiabatic inversion pulse. A phase skip is used to be in control of the inversion efficiency and  
6 inflowing fast blood. The VASO images are acquired around the blood nulling time at  $T11 =$   
7  $1.1$  s after sequential transmission of multi-band RF excitation pulses. The multi-band factor  
8 varies between 2 and 4 in this study (SMS-factor = 4 in figure).  $\Delta T1$  denotes the deviation of  
9 the theoretical blood nulling time. Dependent on the acquisition parameters it is  $\Delta T1 = 75 -$   
10  $175$  ms in this study. The phase-encoding and read gradients for the 2D-EPI acquisition are  
11 accompanied with blipped-CAIPI gradients in slice direction for controlled aliasing of near  
12 slices. In this study the corresponding FoV-shift factor was between 1 and 1/3 (here, FoV-  
13 shift = 1/3). A second set of images is acquired at  $T12 = 2.6$  s containing BOLD signal  
14 weighting without CBV-weighting.

15 **Fig. 2: Results from experiment A: two slice groups during visuo-motor task.**

16 SMS-VASO results for high-resolution imaging of the visuo-motor network containing V1, V5,  
17 M1, and S1. The left side of the figure refers to VASO-CBV sensitivity and the right side  
18 refers to the interleaved acquired BOLD signal. **A** depicts the imaging slab orientation, tSNR  
19 maps and the functional response of one representative subject. It can be seen, how the  
20 insensitivity of VASO to large draining veins results in an improved specificity to GM tissue  
21 compared to BOLD. The purple insets show how the activity clusters of VASO are confined to  
22 the two GM banks of the central sulcus, while BOLD signal shows one connected blob only.  
23 Also in V1, VASO activity patterns can delineate the cortex at the subarachnoid boundary  
24 better compared to GE-BOLD (blue arrow). **B** depicts the stability of the results across four  
25 participants. The higher specificity of VASO to GM tissue of M1 compared to GM tissue of S1  
26 is visible consistently across participants. **C** depicts the corresponding time courses of BOLD  
27 and VASO signal in ROIs of V1, M1, and S1. Note that VASO is a negative contrast and VASO  
28 signal decrease is indicating CBV increase. Error bars refer to inter-participant standard  
29 deviations.

30 **Fig. 3: Results from experiment B: High-resolution imaging of the entire M1/S1 region.**

31 SMS-VASO results for high resolution imaging of the sensory-motor cortex. The left side of  
32 the figure refers to VASO-CBV sensitivity and the right side refers to the BOLD signal  
33 acquired interleaved. **A** depicts the imaging slab orientation, tSNR maps and the functional  
34 response of one representative subject. It can be seen how the insensitivity of VASO to large  
35 draining veins results in an improved specificity to GM tissue compared to BOLD. Activity  
36 clusters of VASO are confined to the two GM banks of the central sulcus, while BOLD signal  
37 shows one connected blob only. Note that the high specificity of VASO to GM tissue  
38 independent of large draining veins clearly reveals that M1 has a higher cortical thickness

1 compared S1, which can be useful in cortical segmentation. **B** depicts the stability of the  
2 results across four participants. The higher specificity of VASO to GM tissue of M1 compared  
3 to GM tissue of S1 is visible consistently across participants. Please note that unlike Fig. 2,  
4 this Fig. does not contain visual areas. The color code is chosen, such that red and blue  
5 stand for activation and deactivation during unilateral finger motion.

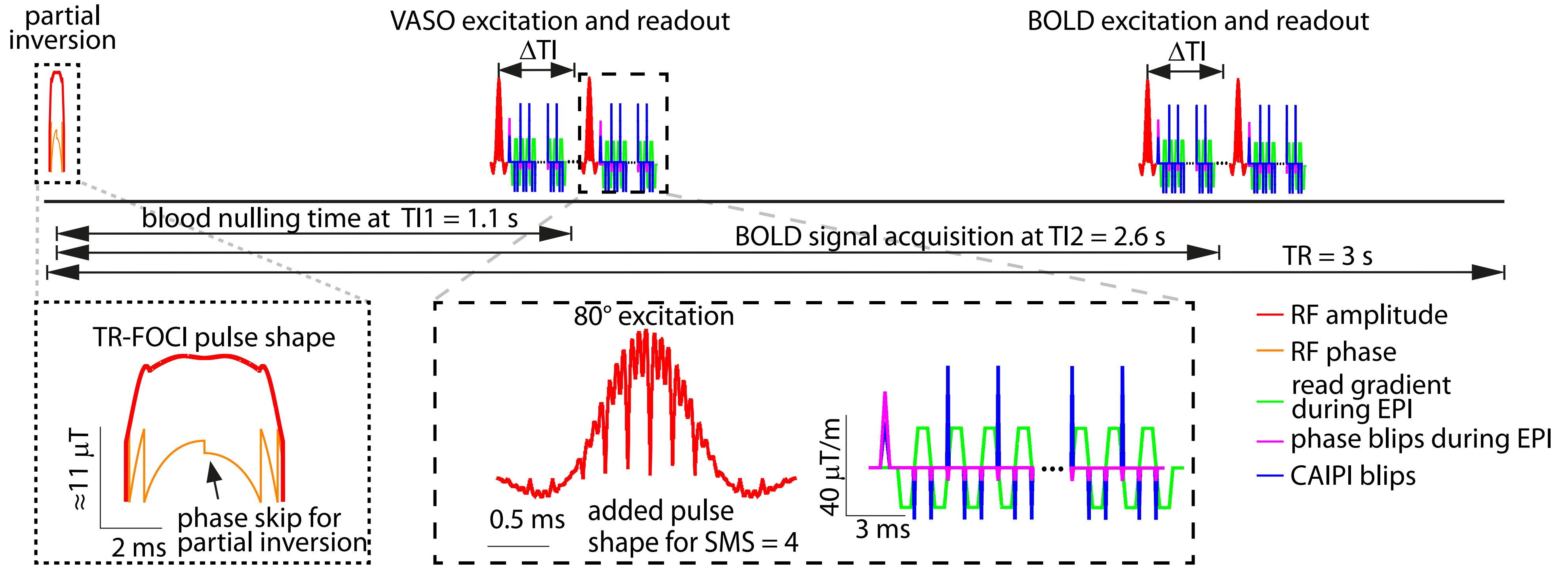
6 **Fig. 4: Results from experiment C: Near whole-brain coverage.**

7 SMS-VASO results for low-resolution near whole-brain coverage. The left side of the figure  
8 refers to VASO-CBV sensitivity and the right side refers to interleaved acquired BOLD signal.  
9 **A** depicts the imaging slab orientation, tSNR maps and the functional response of one  
10 representative subject **B** depicts the stability of the results across four participants. Both,  
11 SMS-VASO and BOLD can detect significant activity in V1, in V5 and the M1/S1 area across  
12 participants.

13

14 **Fig. 5: Direct comparison of SMS-VASO and non-SMS-VASO.**

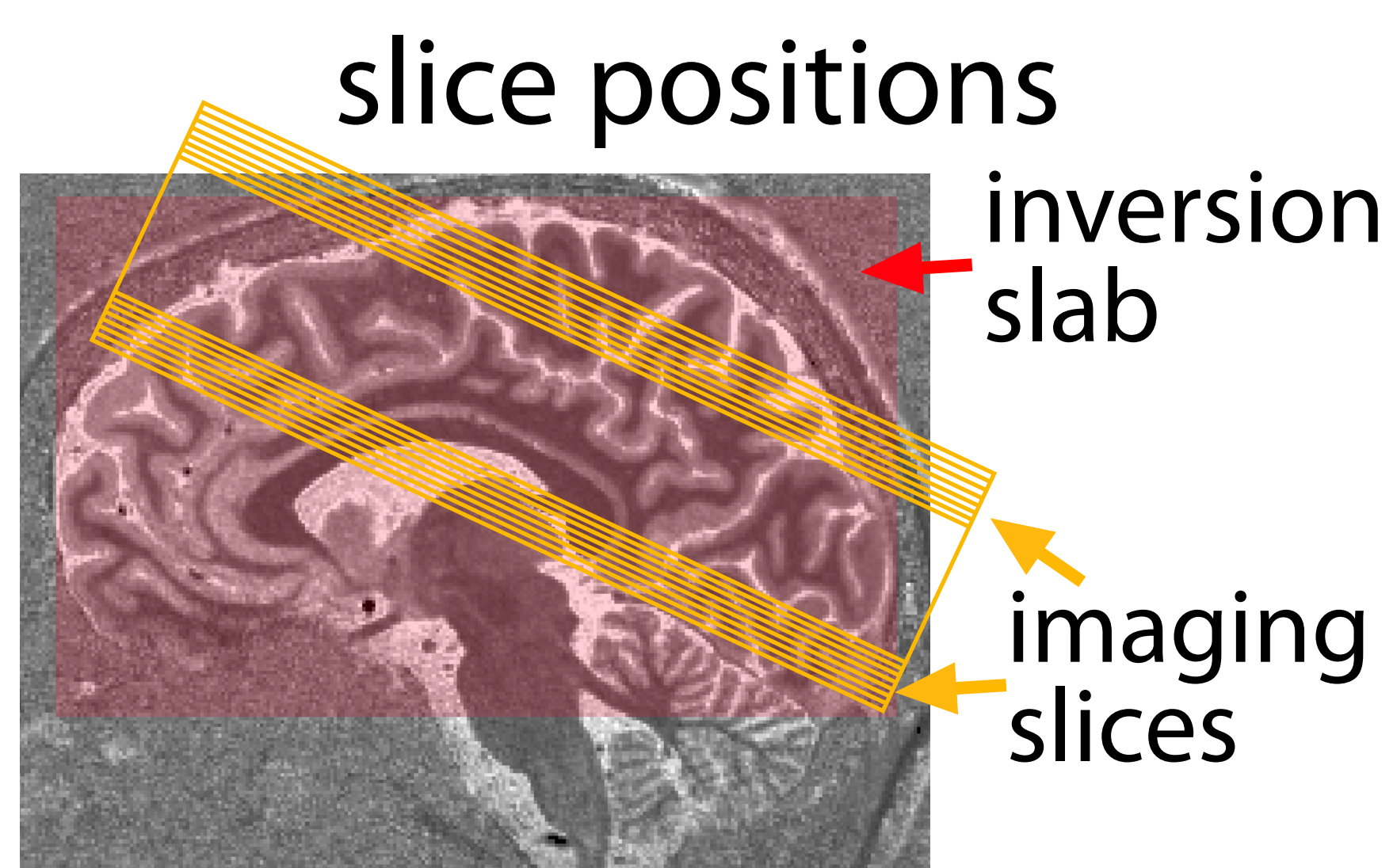
15 tSNR results for all three experimental protocols (A-C) in three participants. tSNR maps with  
16 and without SMS refer to the same in-plane acquisition scheme. There is no apparent loss of  
17 image quality when applying SMS imaging compared to conventional single-band imaging.  
18 With the application of blipped-CAIPI and the leakBlock unaliasing, the tSNR reduction is  
19 below 15% in all protocols and there is no visible signal leakage between the simultaneously  
20 acquired slices.





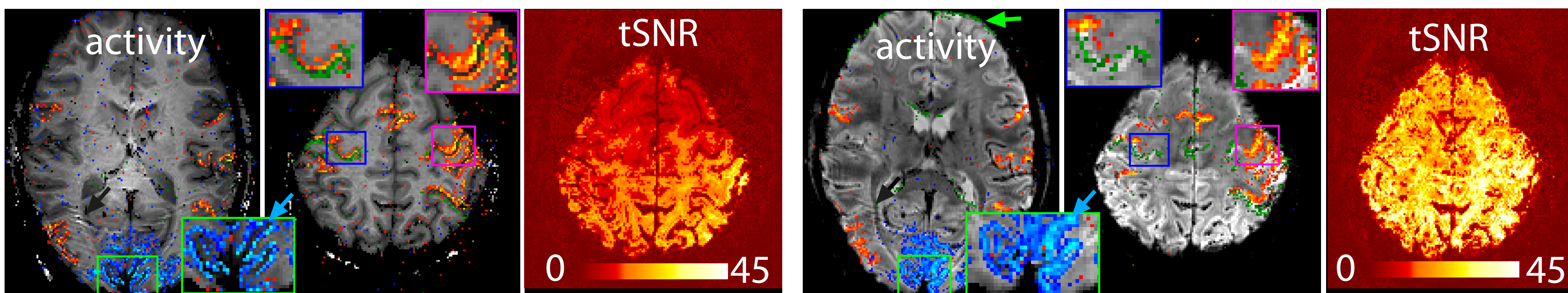
## A representative participant

VASO

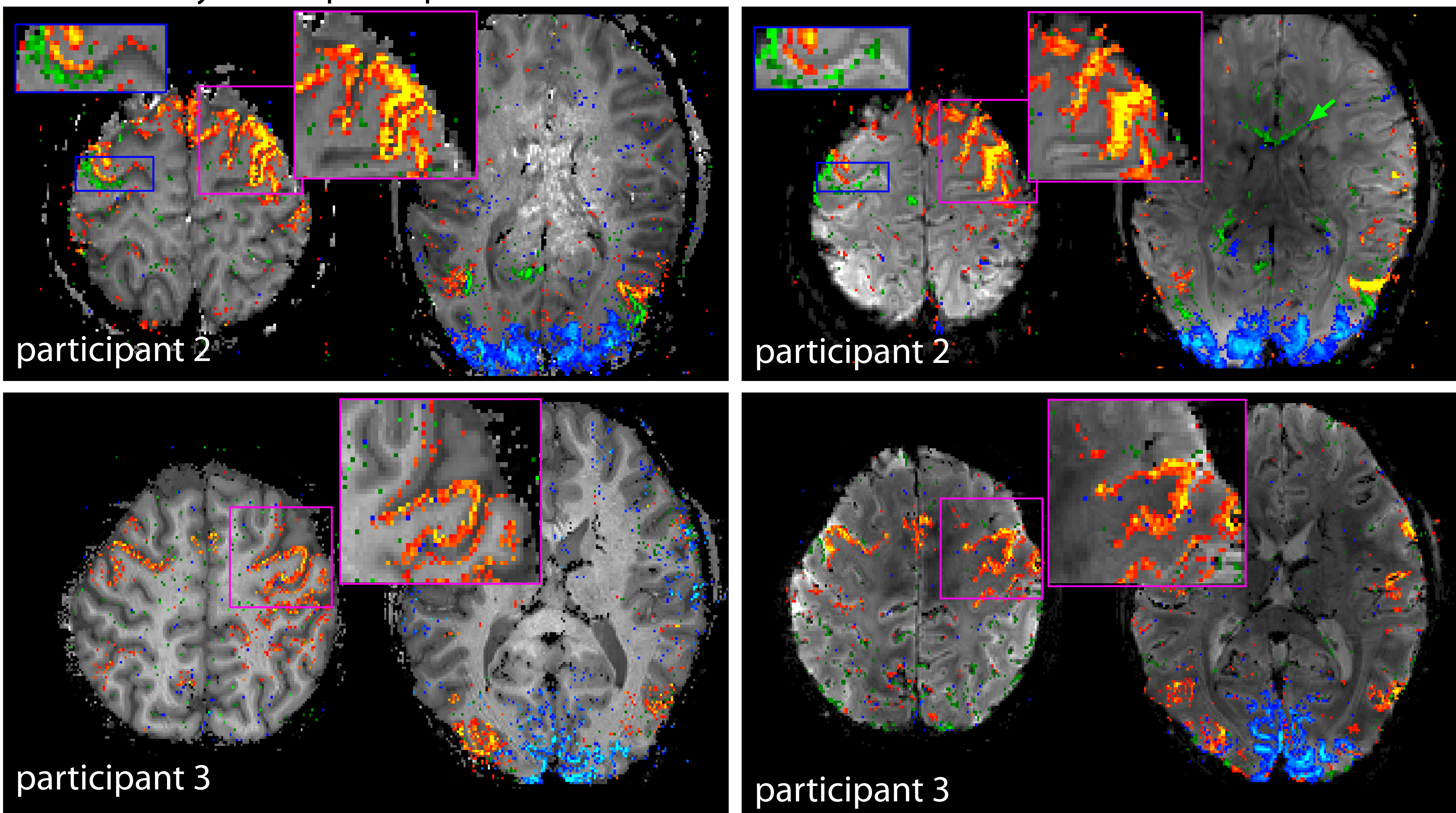


z-val	BOLD 3		static 12 3		motion 20 3		static 12	
	vs.	rest	7	1.7	vs.	static	8	1.7
	VASO 1.7						motion 8	

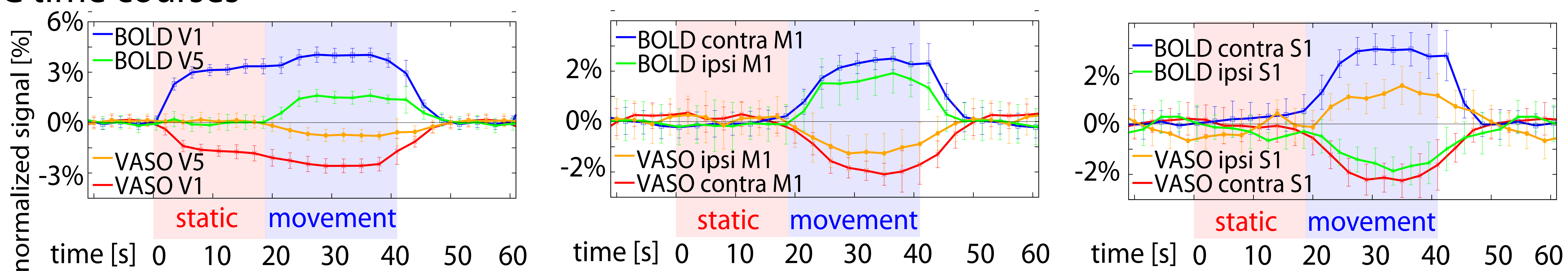
BOLD



## B consistency across participants



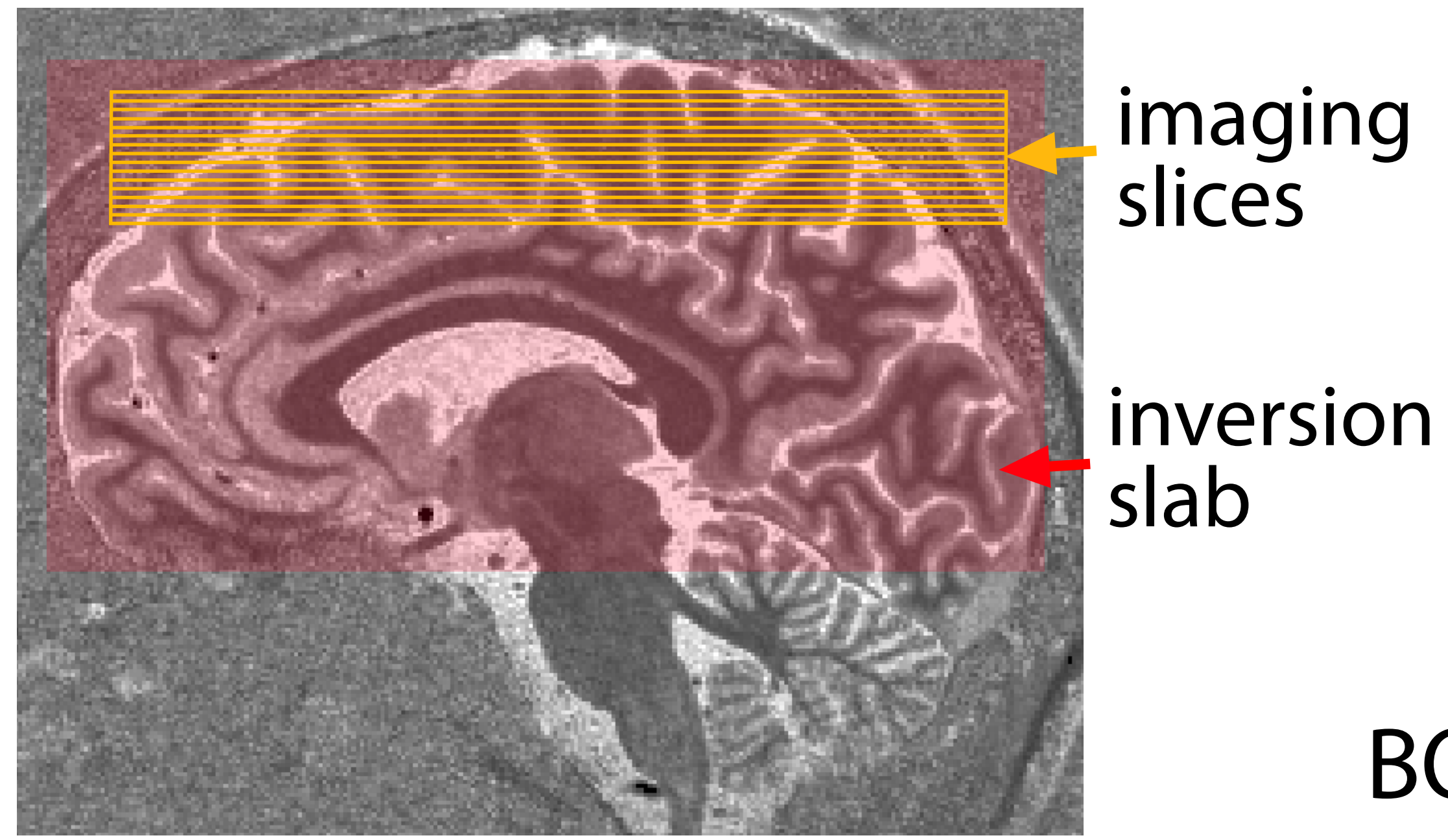
## C time courses





A representative participant

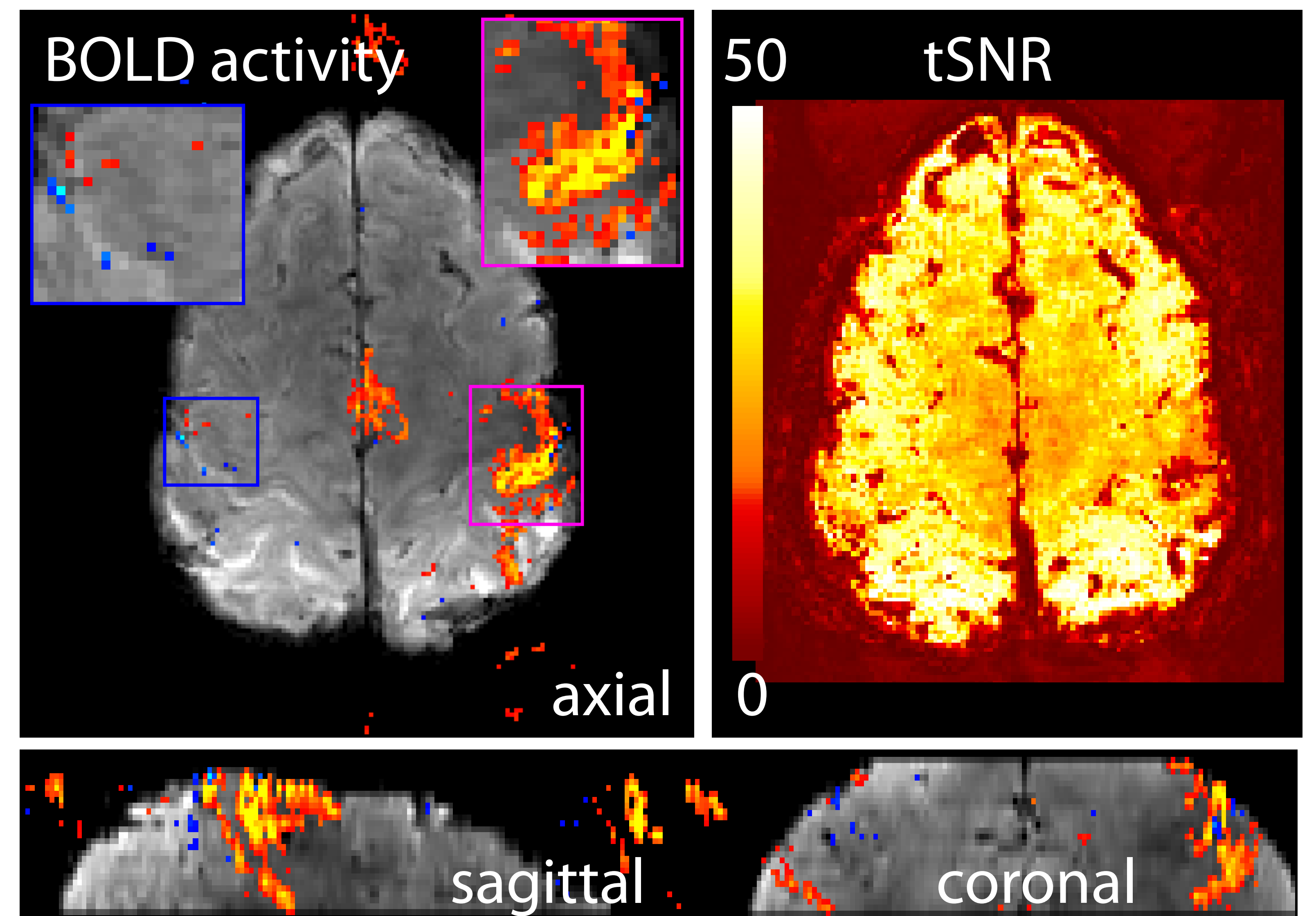
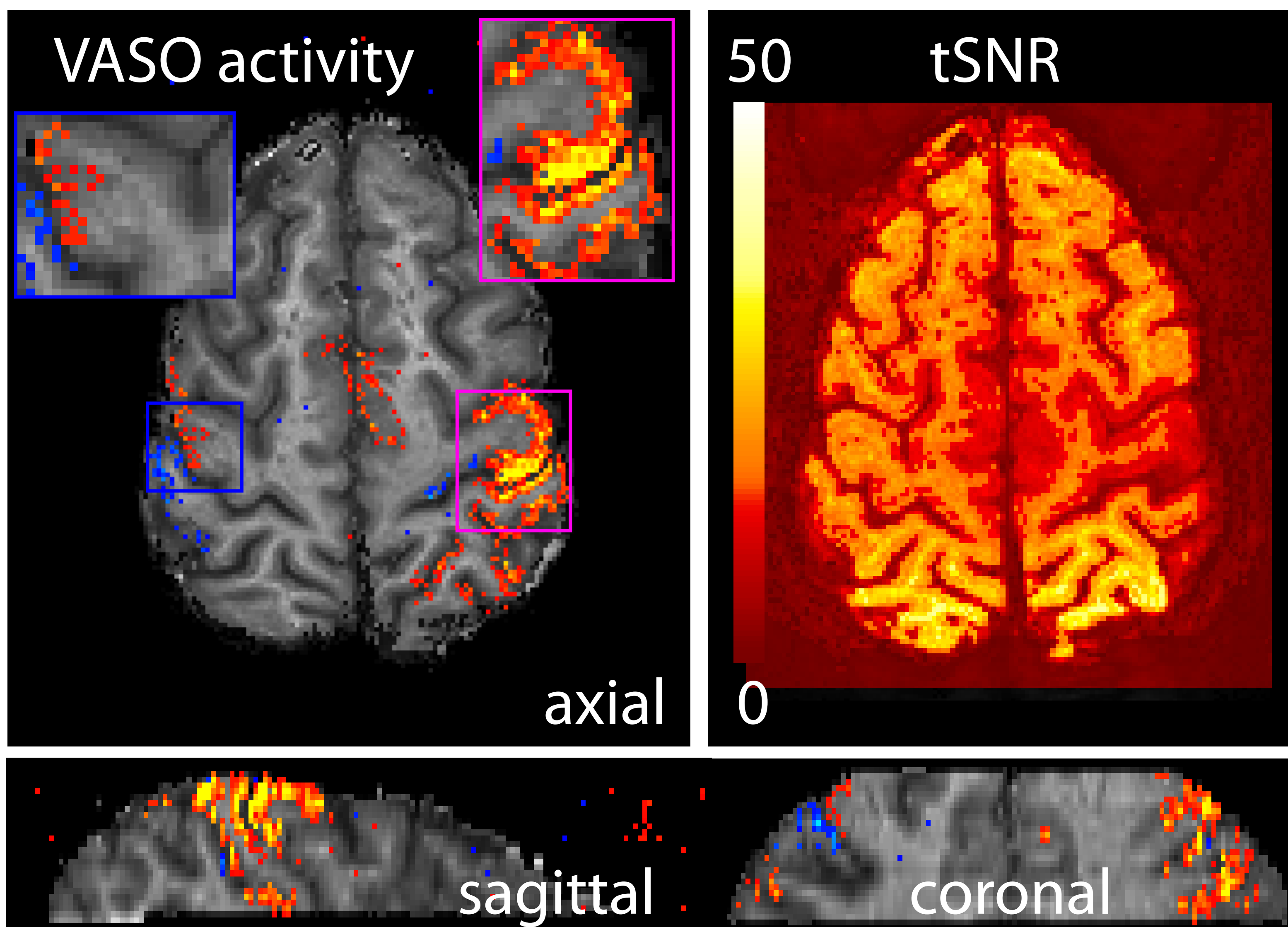
slice positions



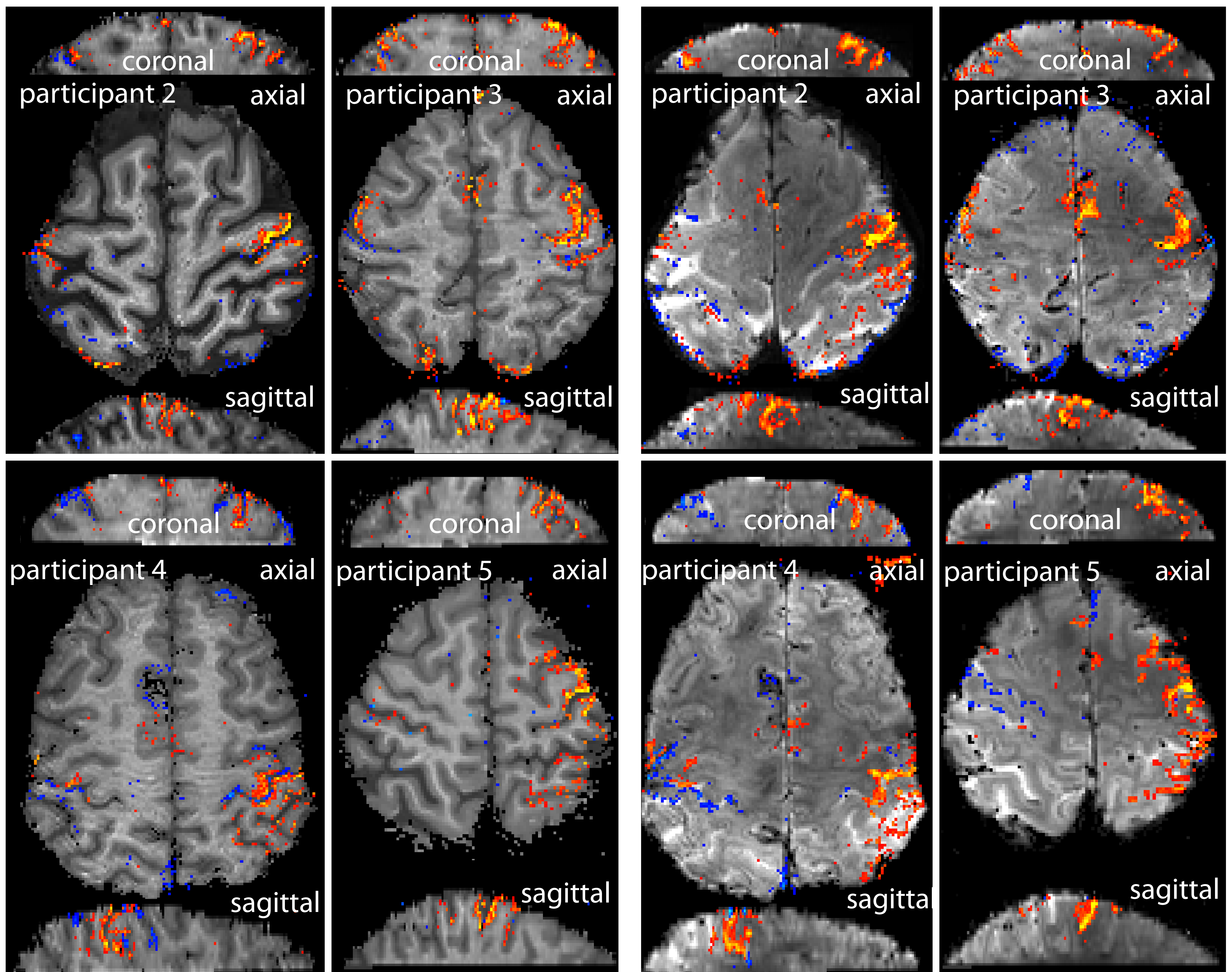
z-val	4	tapping	21	3	rest vs.	8
BOLD	2	vs. rest	9	2	tapping	5
VASO						

VASO

BOLD



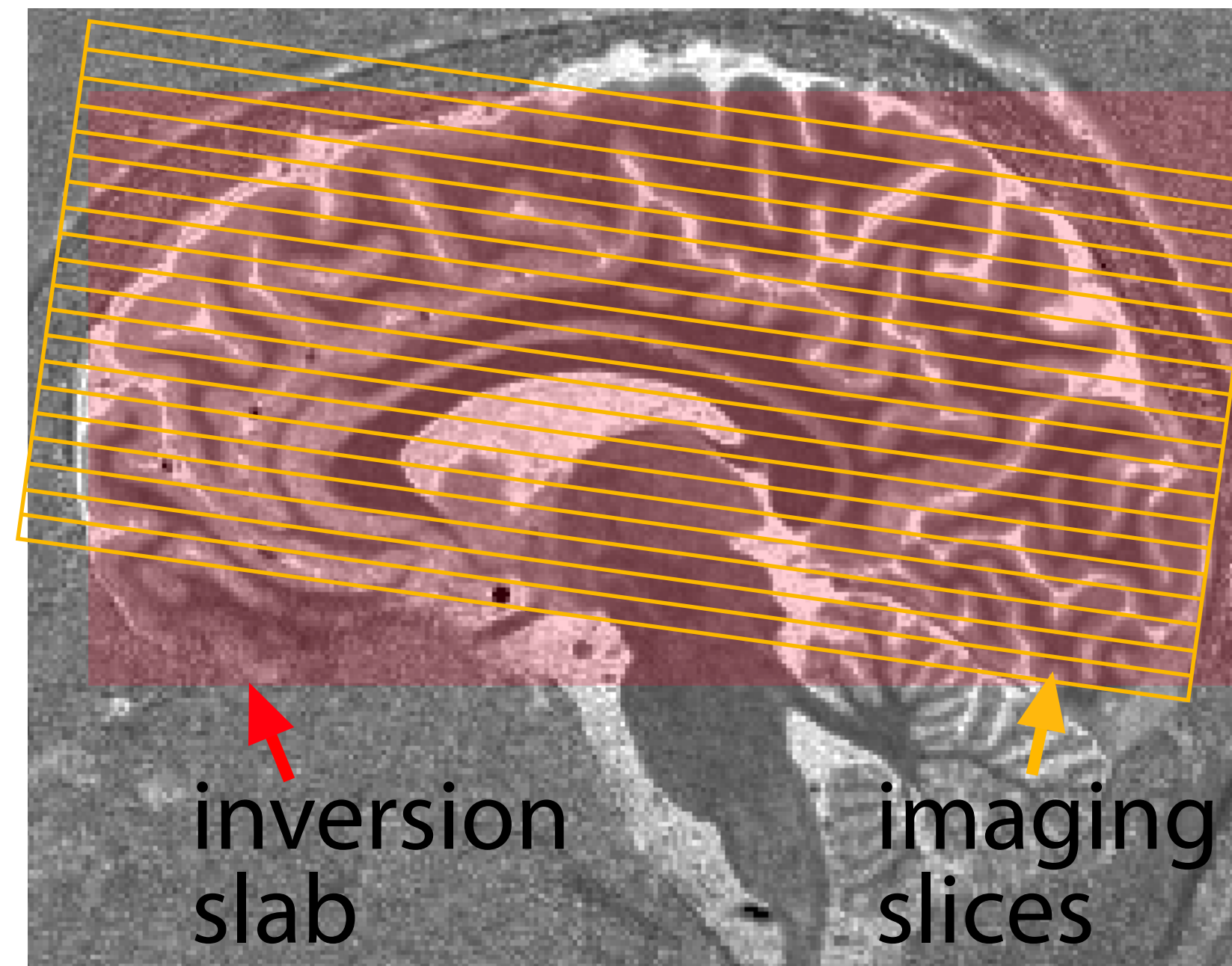
B consistency across participants





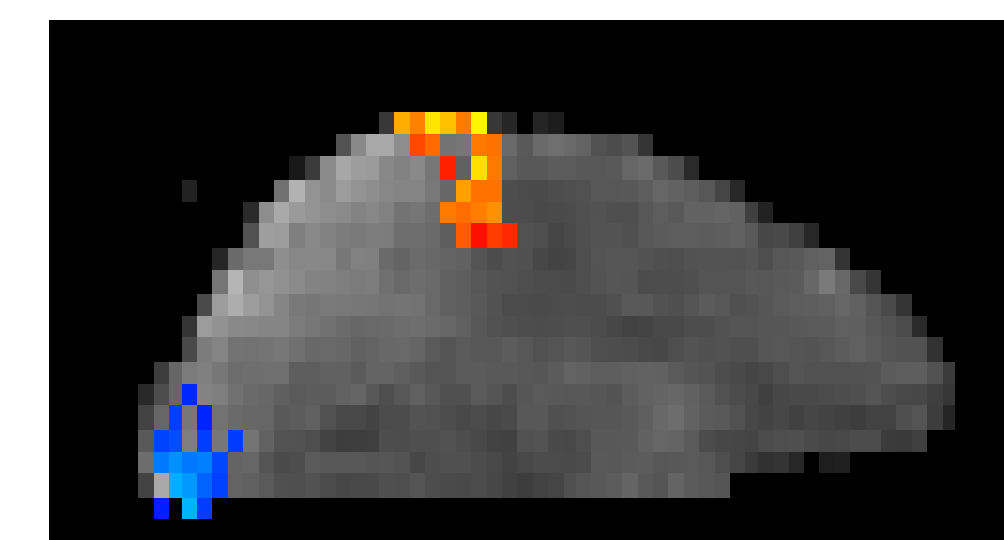
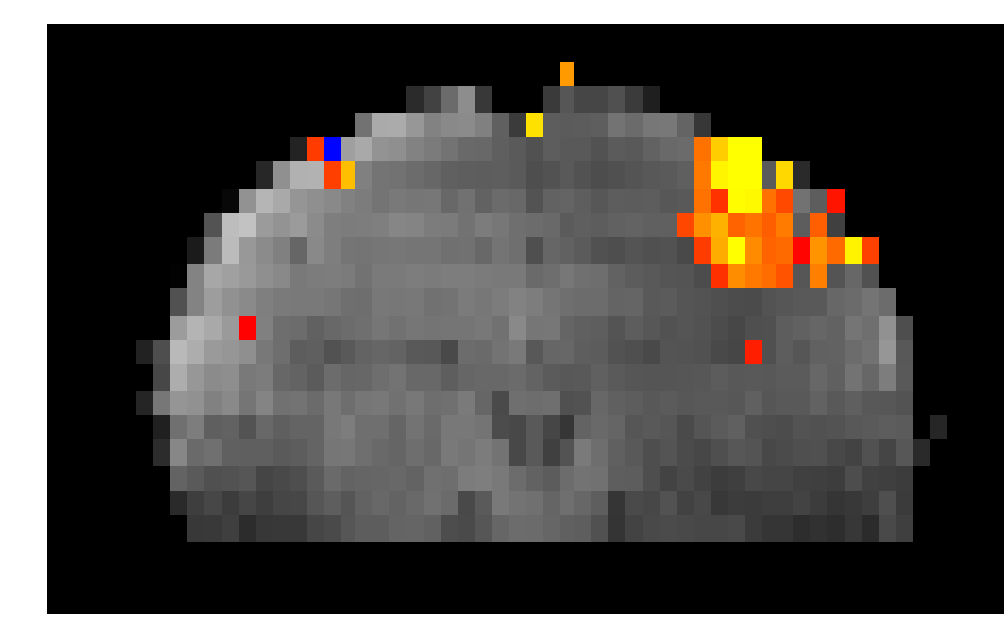
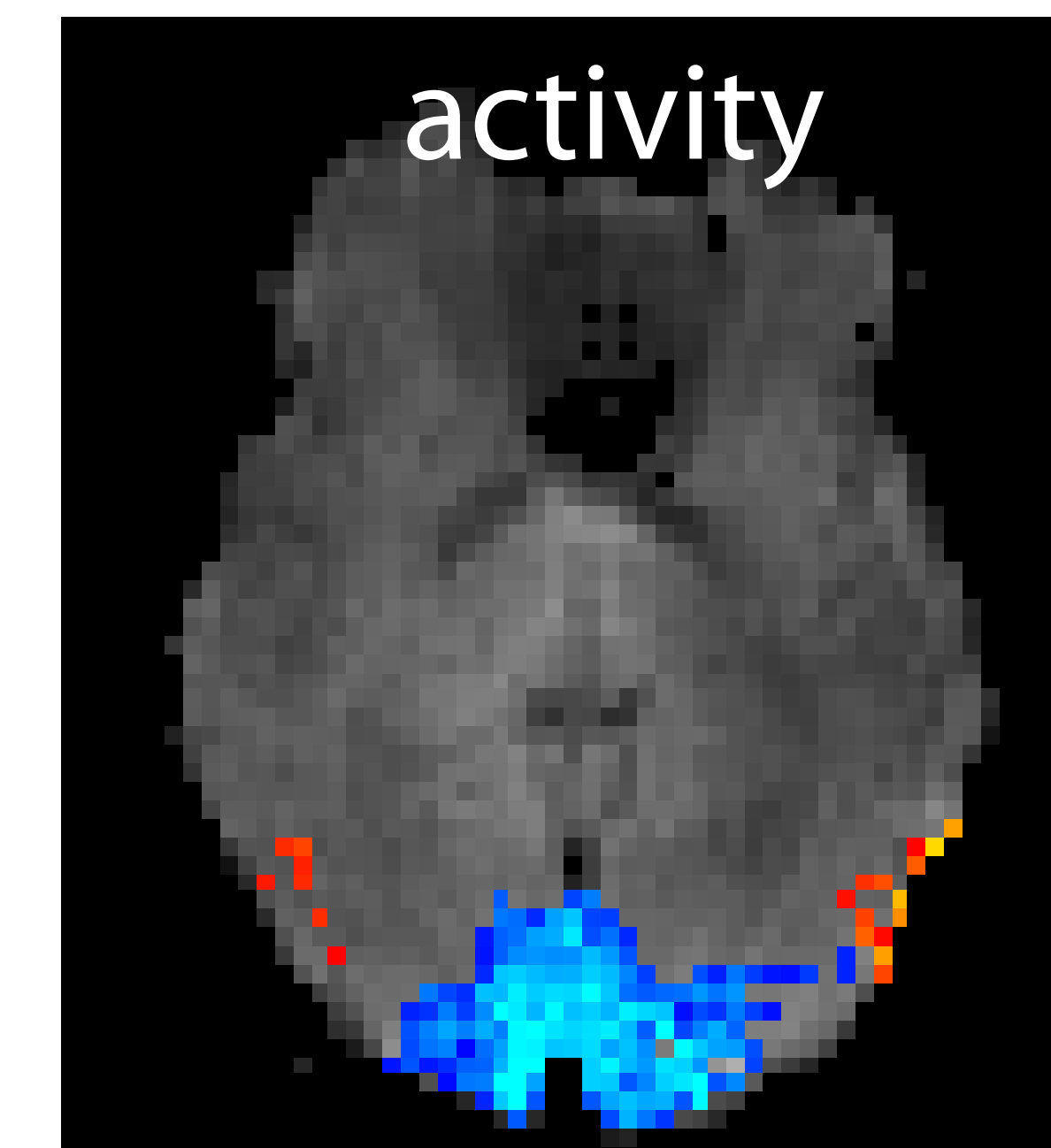
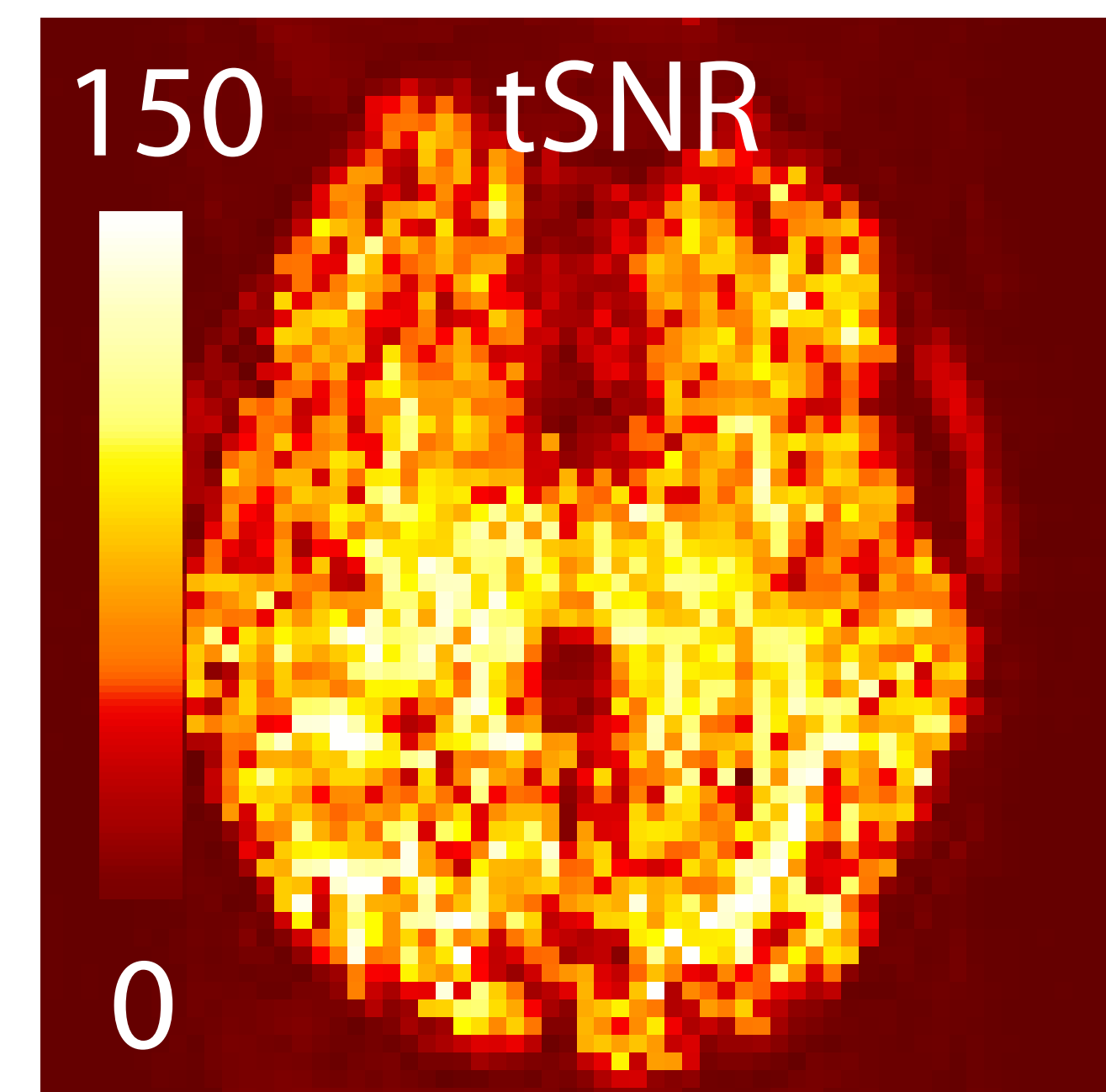
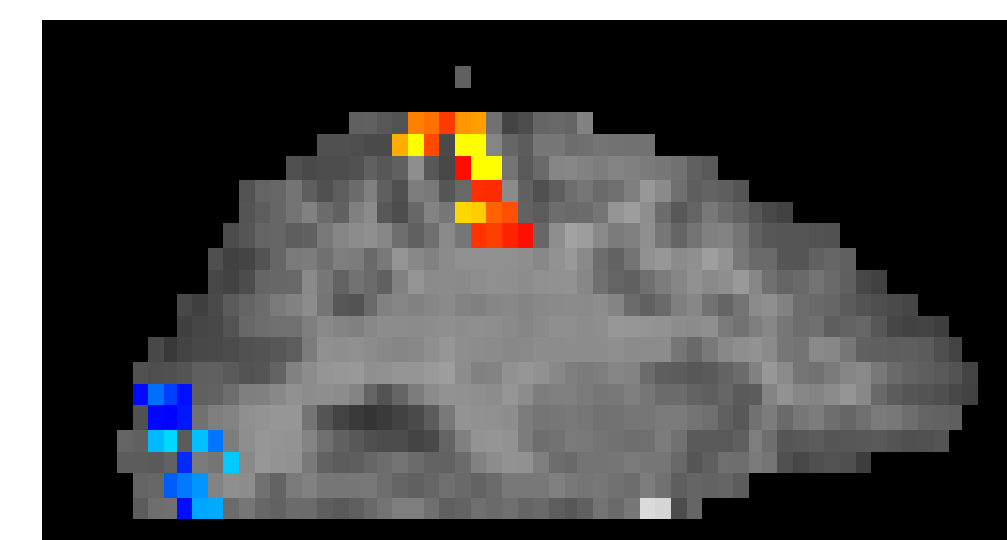
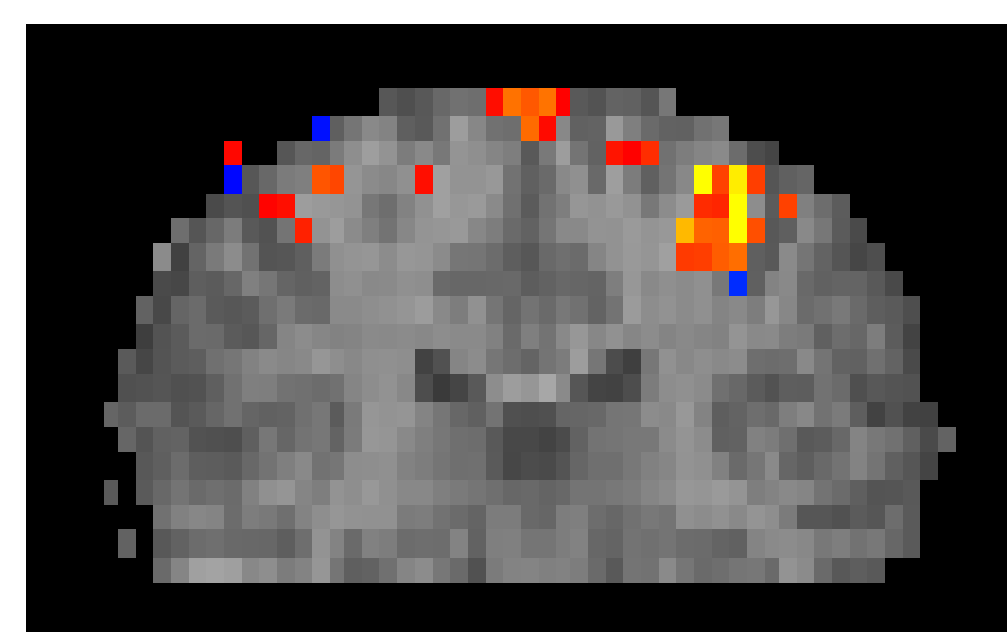
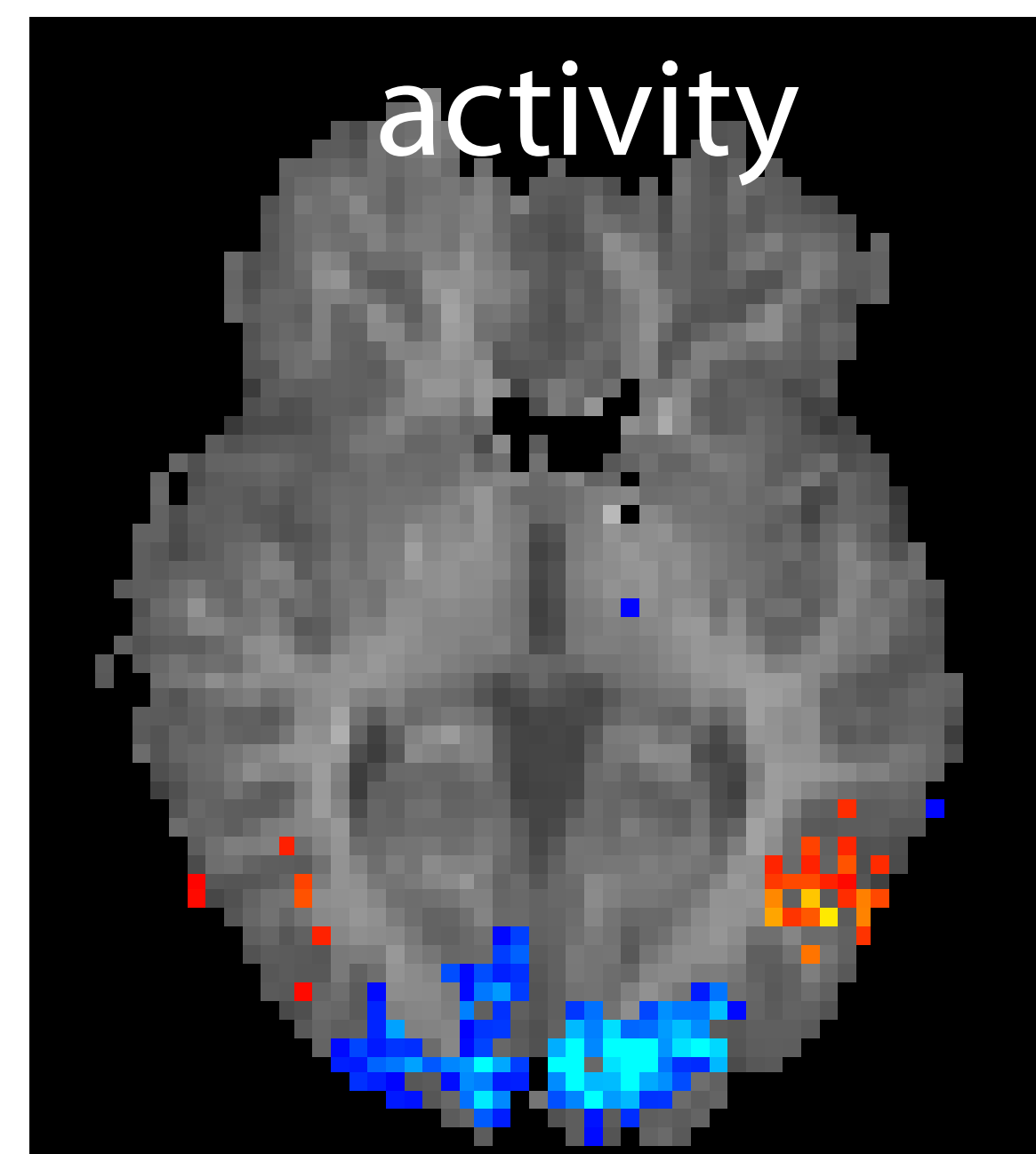
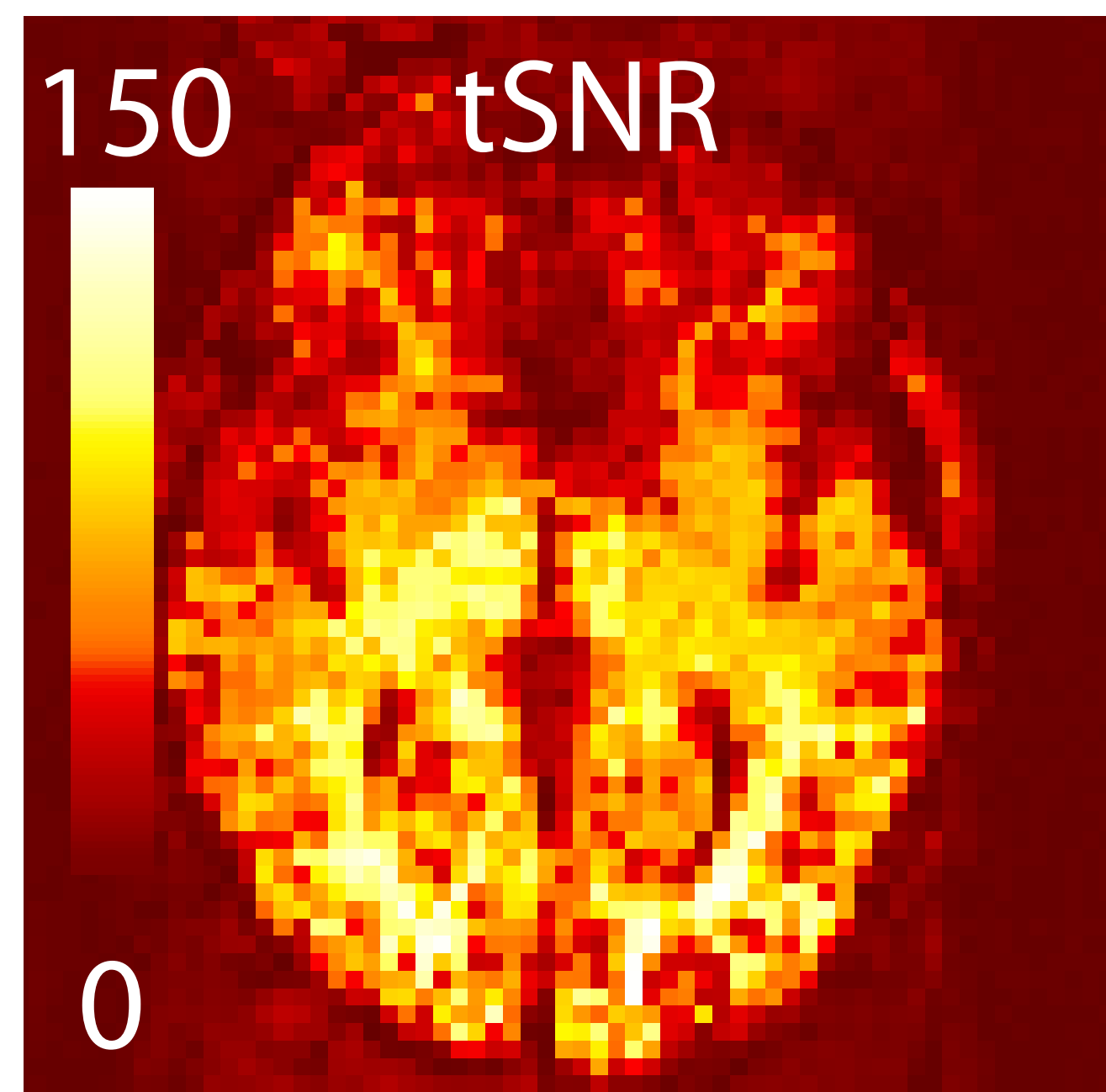
A representative participant

slice positions



VASO

BOLD



B consistency across participants

